Coherent control in femtochemistry

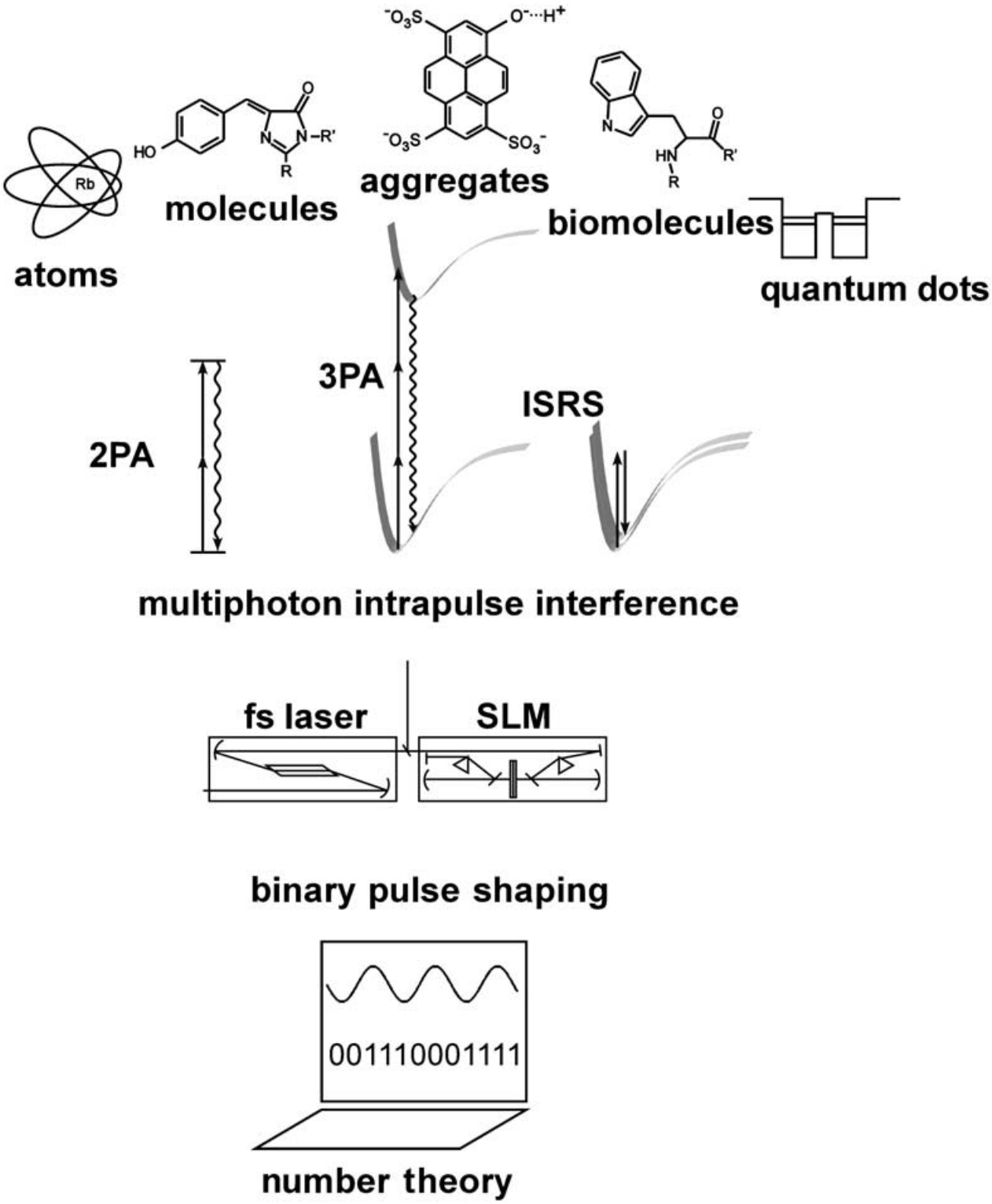

 DOI: 10.1002/cphc.200400342

DOI: 10.1002/cphc.200400342

Systematic Control of Nonlinear Optical Processes Using Optimally Shaped Femtosecond Pulses

Vadim V. Lozovoy[b] and Marcos Dantus*[a]

This article reviews experimental efforts to control multiphoton transitions using shaped femtosecond laser pulses, and it lays out the systematic study being followed by us for elucidating the effect of phase on nonlinear optical laser–molecule interactions. Starting with a brief review of nonlinear optics and how nonlinear optical processes depend on the electric field inducing them, a number of conclusions can be drawn directly from analytical solutions of the equations. From a Taylor expansion of the phase in the frequency domain, we learn that nonlinear optical processes are affected only by the second- and higher-order terms. This simple result has significant implications on how pulse-shaping experiments are to be designed. If the phase is allowed to vary arbitrarily as a continuous function, then an infinite redundancy that arises from the addition of a linear phase function across the spectrum with arbitrary offset and slope could prevent us from carrying out a closed-loop optimization experiment. The early results illustrate how the outcome of a nonlinear optical transition depends on the cooperative action of all frequencies in the bandwidth of a laser pulse. Maximum constructive or destructive interference can be achieved by programming the phase using only two phase values, 0 and π. This assertion has been confirmed experimentally, where binary phase shaping (BPS) was shown to outperform other alternative functions, sometimes by at least on order of magnitude, in controlling multiphoton processes. Here we discuss the solution of a number of nonlinear problems that range from narrowing the second harmonic spectrum of a laser pulse to optimizing the competition between two- and three-photon transitions. This Review explores some present and future applications of pulse shaping and coherent control.

1. Introduction

A number of significant results have been published in which shaped femtosecond pulses were shown to be capable of controlling the outcome of laser-initiated chemical reactions; these seminal contributions have been reviewed elsewhere.[1–10] These results have revitalized the dream of controlling chemical reactivity. Predictable control would have a number of potential applications ranging from clean and efficient chemical synthesis to analytical methods for chemical identification, and even for controlling gates in quantum computers yet to be designed. However, before any of these dreams are realized, robust and reproducible success in this very difficult endeavor requires a more systematic exploration of the nonlinear interaction between phase-modulated laser pulses and matter.

To the best of our knowledge, the first suggestion about the use of shaped pulses in a nonlinear optical application was published in 1984 by Warren.[11] In this theoretical paper, the author analyzed the effect of pulse shaping in the time domain on population inversion near an electronic resonance. The spectrum of the shaped pulse was found to play an important role when choosing the optimal temporal shape to make π or 2π optical pulses (inducing complete population transfer, or no population transfer). In 1987, Warren et al.[12] used the example of nonlinear I_2 excitation to experimentally demonstrate the effect of the shape of a 100–200 ns laser pulse on the induced fluorescence yield.

In 1988, Weiner, Nelson and co-workers published a milestone paper in which multiple-pulse impulsive stimulated Raman scattering (ISRS) was used to selectively drive specific modes in a molecular crystal.[13,14] The train of pulses was generated by a phase-only shaper using an etched mask; the phase was patterned according to a periodic repetition of a pseudo-random binary phase code[15–17] and in the experiments[14] the phase shift of the spectral components was 0.85π to improve the quality of the train. The authors claimed that phase-modulated pulses achieve more efficient excitation of a selected mode in the crystal than transform-limited (TL) pulses, because phase modulation suppresses multiphoton damage.

Binary amplitude modulation (0 and 1 transmission), designed according to Fresnel optics, was introduced in 1992 by Broers et al. to demonstrate spectral focusing of second harmonic generation (SHG) and two-photon absorption (2PA) of Rydberg states in Rubidium.[18–20] The initial quadratic phase distortion (chirp) on the pulses was cancelled by means of re-

[a] *Prof. Dr. M. Dantus*
Department of Chemistry and Department of Physics and Astronomy
Michigan State University, East Lansing, MI 48824 (USA)
Fax: (1) 517-353-1793
E-mail: dantus@msu.edu

[b] *Prof. Dr. V. V. Lozovoy*
Department of Chemistry
Michigan State University, East Lansing, MI 48824 (USA)

moving from the spectrum those components which gave destructive interference.

In 1992, Judson and Rabitz suggested the use of learning algorithms to optimize the phase and amplitude of femtosecond pulses to control optical processes.[21] Feedback quantum control of energy transfer in molecular systems was experimentally implemented for the first time in 1997.[22] Since that time, many experiments based on a feedback-optimized genetic algorithm (GA) for control of different nonlinear optical process have been reported. Optimization of SHG has received the most attention (see results by the Silberberg and co-workers,[23–25] Gerber and co-workers,[26–28] Reitze and co-workers,[29–32] Kannari and co-workers,[33–35] Murnane, Kapteyn and co-workers,[36,37] Motzkus and co-workers,[38] Miller and co-workers,[39,40] Baltuska and Kobayashi,[41,42] Corkum and co-workers[43] and Keller and co-workers[44–46]). Subsequent applications include control of chemical reaction yields,[47–56] 2PA in isolated atoms[57–59] and in complex solutions,[60,61] energy distribution in small molecules,[62–65] polymers,[66] and bio-molecular complexes,[67] high harmonic generation,[68] cluster photochemistry,[69,70] nonlinearity in condensed phase,[71] transmission through optical fibers,[72] semiconductor nonlinearities,[73] and four-wave mixing.[74] This is a very wide range of applications, and in each particular case some degree of success was reported. Despite these successes it is difficult and in some cases impossible to determine if a better solution exists. For this reason we have carried out a systematic approach presented herein.

In 1998, Meshulach and Silberberg demonstrated that femtosecond laser pulses can be tailored, using phase shaping techniques, to control 2PA in cesium using pulse-shaping techniques.[75] In this paper the authors showed that symmetrical phase modulation cancelled the transitions due to destructive interference, while antisymmetric modulation did not strongly affect the 2PA. In a subsequent paper,[76] the authors analyzed the effect of pulse shapes on *N*-photon absorption as well as on Raman transitions and showed theoretically that certain tailored pulses do not excite the system, while other shaped pulses induce transitions as effectively as transform-limited pulses. A spectral phase step (π jump) was scanned across the laser pulse spectrum. When the phase step crossed the center of the pulse spectrum, the two-photon excitation of Cs exhibited a sharp increase to a level that was as intense as that produced by excitation with transform-limited (TL) pulses. When the experiment was repeated for coumarin 6H, a large molecule in methanol solution, this sharp increase was not seen. This observation implied that the sharp resonance method conceived by Silberberg failed in the cases involving broadband absorption, such as is common in large molecules in solution.

In a paper published in 1999, Wilson and co-workers experimentally demonstrated the use of chirp-condition-dependent fluorescence yield to distinguish among different molecules or the same molecules in different micro-environments.[77]

In a series of papers published in the years 1999–2001, Zheng, Weiner and co-workers demonstrated coherent control of second harmonic generation, obtaining contrast of more than three orders of magnitude. The two-photon photocurrent of a GaAs/AlGaAs diode was strongly suppressed by means of pseudo-random phase shaping.[78] In the succeeding papers[78,79] the authors used thick, periodically poled, nonlinear crystals to generate a second harmonic output in narrow phase-matching conditions. The spectral phase was binary coded (0 or π phases) in the low- and high-frequency ends of the spectrum with *M*-sequences or Hadamard codes and it was shown that if the codes in the left and right sides are not the

Vadim V. Lozovoy was born in Novosibirsk, USSR. He received his MS degree in physics from Novosibirsk State University, where he studied reactions of ion radicals with optically detected electron spin resonance spectroscopy and positron annihilation. He received his Ph.D. degrees in physics and mathematics from the Institute of Chemical Kinetics and Combustion in 1989. His dissertation research involved the discovery of fast energy transfer by excitons in liquid cyclic hydrocarbons using picosecond pulse radiolysis. In 1991 he worked at the N.N. Semenov Institute of Chemical Physics were he designed and constructed a femtosecond spectroscopy laboratory. He conducted a number of experiments on ultrafast coherent chemical dynamics. In 1999 he moved to Michigan State University, where he has studied, experimentally and theoretically, laser control of intramolecular dynamics with four-wave mixing spectroscopy. His present work, as an Assistant Research Professor at MSU, concerns the theory of coherent laser control. He has published 61 scientific papers, reviews, and patents.

Professor Marcos Dantus was born in Mexico. He received B.A. and M.A. degrees from Brandeis University and a Ph.D. degree in Chemistry from Caltech under the direction of Professor Ahmed H. Zewail. His Ph.D. work focused on the development of femtosecond transition-state spectroscopy, and his postdoctoral work on the development of ultrafast electron diffraction. He is presently a Professor of Chemistry and Adjunct Professor in Physics at Michigan State University. Professor Dantus has received many honors and awards. He received the Milton and Francis Clauser Doctoral Prize (for the most significant Ph.D. thesis) from Caltech. In 1992, he was honored with the Nobel Laureate Signature Award for Graduate Education in Chemistry. He received the Beckman Young Investigator Award, the Packard Fellowship for Science and Engineering, the Eli Lilly Teaching Fellowship, the Alfred P. Sloan Research Fellowship, and the Camille Dreyfus Teacher-Scholar Award. Dantus' research interests include ultrafast dynamics, coherent laser control of laser–matter interactions, and quantum computation. Professor Dantus has published 84 scientific articles, and 4 patents.

same, then the intensity is suppressed by a few orders of magnitude.[80,81]

In 2001, Hacker et al. investigated theoretically (analytically) and experimentally the SHG from a thin crystal for sinusoidally shaped pulses. Their results showed that fundamental phase modulation can be translated into an amplitude spectral modulation of the SHG.[82]

In 2001, Silberberg and co-workers[83,84] experimentally and theoretically demonstrated that interference between resonant and nonresonant contributions in two-photon excitation can be destructive and constructive. Using amplitude blocking and a step-function phase modulation it was possible to increase the fluorescence from two-photon excited Rb atoms by several times. Later, Leone and co-workers used feedback and evolutionary algorithms with a phase shaper to optimize the interference between resonant and nonresonant contributions to multiphoton excitation of Li_2.[85]

In a series of papers published in 2002–2003, Silberberg and co-workers studied the effects of phase-shaped pulses on coherent anti-Stokes Raman scattering (CARS) spectroscopy. The authors used a sharp phase step[86] or phase gate[87] to induce sharp Raman resonances in solids and liquids. By shaping both the pump and the Stokes pulses with gate step-phase functions, the authors eliminated the nonresonant CARS signals and achieved selective excitation of one of the two neighboring energy levels of pyridine.[88] In the following papers the authors used a combination of resonance–non-resonance interference with periodical phase modulation (sinusoids and harmonics) to improve the resolution of resonance CARS spectroscopy in the fingerprint region of several solids and liquids[89] and by imaging capillaries filled with CH_2Br_2.[89] The same group used polarization shaping to better suppress the background signal in CARS[90] and to control two-photon absorption in Rb.[91] Recently a periodic-step spectral phase modulation has been used by Faucher and co-workers to selectively excite odd or even rotational states in N_2 trough ISRS.[92]

Our group initially concentrated on methods that took into account intramolecular dynamics to achieve controlled ground- or excited-state wave packet preparation in molecules.[93,94] In 2001, we began to explore the laser pulse requirements for controlling the multiphoton excitation of large organic molecules in solution. We initially used a sine function to cause interference between pairs of frequencies within the bandwidth of the laser during multiphoton transitions. We demonstrated that multiphoton intrapulse interference (MII) could be used to control the multiphoton excitation of large molecules, including proteins, in solution, and to control two- versus three-photon excitation.[95,96] We used MII to enhance the amplitude of the nonlinear field at specific frequencies and to suppress the nonlinear field amplitude elsewhere. This technique enables us to show robust and reproducible control of nonlinear optical transitions and to demonstrate selective two-photon microscopy. Selective two-photon excitation was accomplished by taking advantage of the difference in two-photon cross-sections of molecules or the effect that the microchemical environment has on specially sensitive chromophores.[97,98] We have used MII to develop a new method of functional imaging in two-photon microscopy.[99] We recognized that the success of MII experiments depended on having a sufficiently large spectral bandwidth. We introduced a technique to characterize and compensate the spectral phase of femtosecond pulses, now known as multiphoton intrapulse interference phase scan (MIIPS),[98,100] and have used this technique to shape pulses as short as 9 fs with a bandwidth of 110 nm full width at half maximum (FWHM). We have shown that complex binary phase functions outperform arbitrary phase functions and amplitude functions in the optimization of multiphoton excitation tasks.[101] More recently, we demonstrated functional imaging through one millimeter biological tissue using binary phase-shaped laser pulses.[102] This experiment gives indication of the future value of pulse shaping for future biomedical applications.

Herein, we review our progress in establishing guidelines that can be used to understand coherent control experiments where a pulse shaper is implemented to manipulate the electric field that interacts with the molecules. This Review is not comprehensive but focuses on theoretical and conceptual extension of our work addressing coherent control in weak and intermediate laser intensity regimes, although, some of the ideas developed here have been applied in strong-field experiments as well, with applications in analytical chemistry.[103] In all examples we assume the pulse shaper as a device, such as a spatial light modulator at the Fourier plane, that can introduce very accurate phase retardation at specific frequency components of the pulse.

In Section 2, we provide the theoretical background of our studies, followed by a brief section on nonlinear optical processes which will indicate similarities among different processes and develop the language that is used throughout the rest of the article. In Section 3, we analyze the effect of phase modulation on the nonlinear components of the electric field starting with second-order processes without an intermediate resonance. We systematically explore the order of spectral phase modulation that is required to affect nonlinear optical processes starting from linear, and moving to quadratic and cubic frequency dependence. We explore the sine function and explore its advantages and disadvantages. In Section 4 we consider the optimum phase modulation required to control multiphoton transitions and introduce binary pulse shaping, based on the principles outlined above. We explore in Section 5 the use of evolutionary learning algorithms in the optimization of nonlinear optical processes, such as 2PA, 3PA, and ISRS. In Section 6, we discuss the structure of the search parameter space and consider the most efficient search methods aimed at maintaining the highest spectral resolution (maximum number of pixels), for a number of cases such as selective 2PA and ISRS. Finally, we conclude with a perspective on present (Section 7) and future (Section 8) applications of these powerful methods. Conclusions are drawn in Section 9.

2. The Effect of Phase Modulation on Nonlinear Processes

In this section, we consider the effects of phase modulation on nonlinear processes. The goal is to establish a connection between different representations of nonlinear optics and equations that can be used to calculate the effect, phase modulation has over the entire spectrum of the pulse, not over a single frequency as has been considered by Silberberg and co-workers[75] and Weiner and co-workers.[80] We start by presenting a general methodology for obtaining expressions for nonlinear optical processes starting from a diagrammatic representation. We emphasize the similarities between SHG, 2PA, and ISRS.

The nonlinear optical material response can be described by expressing the polarization, the dipole moment per unit volume [see Eq. (1)], $P(t)$, as a power series in the electric field strength $E(t)$:[104–106]

$$P(t) = \chi^{(1)} E(t) + \chi^{(2)} E^2(t) + \chi^{(3)} E^3(t) + \ldots \equiv P^{(1)}(t) + P^{(2)}(t) + P^{(3)}(t) + \ldots \quad (1)$$

where the quantities $\chi^{(n)}$ are known as the tensors of nth-order nonlinear optical susceptibilities. In the dipole approximation, when the size of the object being polarized is smaller than the wavelength of light, and under perturbative approximation (relatively weak interaction), we can write Equation (2)[107]:

$$P^{(n)}(t) = \int \mathrm{d}t_n \int \mathrm{d}t_{n-1} \ldots \int \mathrm{d}t_1 \, S^{(n)}(t, t_n, t_{n-1}, \ldots t_1) \, E(t-t_n) \, E(t-t_n-t_{n-1}) \cdots E(t-t_n-t_{n-1} \ldots -t_1) \quad (2)$$

The nth-order nonlinear response function $S^{(n)}$, carries the complete microscopic information necessary for the calculation of optical measurements,[107] but in most cases it is difficult to calculate, even when the Hamiltonian of the system is known. The nonlinear polarization $P(t)$ and the field $E(t)$ are physically measurable real quantities and can be written as sum of complex oscillatory components with carrier frequency ω_0 [Eq.(3)]:

$$F(t) \equiv F(t)e^{-i\omega_0 t} + F^*(t)e^{i\omega_0 t} \quad (3)$$

For most cases in femtosecond spectroscopy the rotating wave approximation is applicable and we can replace the real field $E(t)$ with only one complex part (the other is just the complex conjugate). Transforming Equation (2) to the frequency domain gives the polarization in the frequency domain as shown in Equation (4)[107]

$$P^{(n)}(\omega_s) = \frac{n!}{(2\pi)^{n-1}} \int \mathrm{d}\omega_1' \ldots \int \mathrm{d}\omega_n' \delta(\omega_s - \omega_s') \chi^{(n)}(-\omega_s', \omega_1', \ldots \omega_n') E(\omega_1') \ldots E(\omega_n') \quad (4)$$

where $E(\omega)$ is complex spectral amplitude of electric field and $\omega_s = \omega_1 + \omega_2 + \ldots + \omega_n$. The number of terms in Equation (4) for an nth-order process grows exponentially due to the various Liouville space pathways and their combinations and permutations that are induced by the field. Diagrammatic representations, such as double-sided Feynman diagrams,[106] Liouville space coupling diagrams,[107] and energy ladder diagrams,[108] are very useful to keep track of nonlinear optical processes. In Figure 1 we present the relevant ladder diagrams of the nonlinear optical processes discussed herein: a) SHG, b) 2PA, c) 3PA, d) ISRS which can be considered the first half of the CARS measurement, e) CARS, f) photon echo.

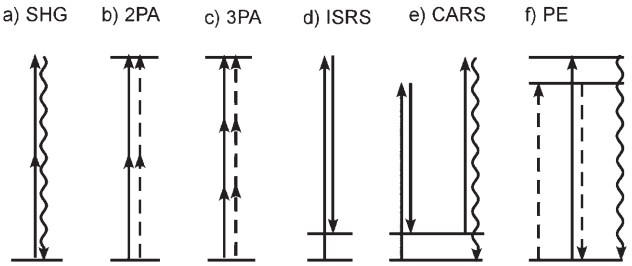

Figure 1. Ladder diagrams of some multiphoton processes; a) second harmonic generation, b) two-photon absorption, c) three-photon absorption, d) impulsive stimulated Raman scattering, e) coherent anti-Stokes Raman scattering, f) photon echo. The dashed and solid lines indicate action of the electric field on the *bra* and *ket*, respectively (see ref. [107]).

Multiphoton processes without intermediate resonance(s) depend on the nonlinear amplitude of the field defined in the time domain as Equation (5):

$$E^{(n-m)}(t) \equiv E^n(t) \, E^{*m}(t) \quad (5)$$

where the n–mth nonlinear optical process depends on the product of the nth-order field times the complex conjugate of the mth-order electric field. The solid arrows in the diagrams shown in Figure 1 correspond to $n e^{-i\omega t}$ interactions (photon annihilation or *bra* interaction) and are given by E^n while the dashed arrows correspond to $m e^{i\omega t}$ interactions (photon creation or *ket* interaction) and are given by E^{*m} in Equation (5). The Fourier image of this field defines the spectral amplitude of effective nonlinear electric field given in Equation (6):

$$E^{(n-m)}(\omega) = \int E^{(n-m)}(t) \, e^{i\omega t} \, \mathrm{d}t \quad (6)$$

The probability of one-photon processes does not depend on the spectral phase of the field, but only on the spectral power at the resonance frequency $|E(\omega)|^2$. To calculate the spectrum of the effective nonlinear electric field given by Equation (6) we use the convolution theorem, which says that the Fourier image of convolution is the product of the Fourier images of the functions. For two-photon processes, Equations (7) and (8) for the effective field are intuitively clear:

$$E^{(2)}(\omega) \propto \int E(t) \, E(t) \, e^{i\omega t} \, \mathrm{d}t = \int E(\Omega) \, E(\omega - \Omega) \, \mathrm{d}\Omega \quad (7)$$

$$E^{(1-1)}(\omega) \propto \int E(t)\,E^*(t)\,e^{i\omega t}\,\mathrm{d}t = \int E(\Omega)\,E^*(\Omega-\omega)\,\mathrm{d}\Omega \qquad (8)$$

where Ω is the detuning of frequency component in the pulse. It is interesting that the spectrum of the effective field for 2PA and ISRS can be written as a self-convolution or an autocorrelation of the fundamental field.

For multiphoton effects with higher orders we can obtain the spectral intensity of the effective field, determined in Equation (9), using Fourier transformation of the time-dependent field:

$$E^{(n-m)}(\omega) \propto \int |E(t)|^{n+m} \exp[i((n-m)\phi(t) + \omega t)]\mathrm{d}t \qquad (9)$$

If we know the spectrum of the field, we can obtain an equivalent expression using the convolution theorem [Eq. (10)]:

$$E^{(n-m)}(\omega) \propto \int \ldots \int E(\Omega_1)\cdots E(\Omega_n)E^*(\Omega_{n+1})\ldots E^*(\Omega_{n+m-1})$$
$$E^*(\Omega_1 + \ldots \Omega_n - \Omega_{n+1} \ldots - \Omega_{n+m-1} - \omega)\mathrm{d}\Omega_1 \ldots \mathrm{d}\Omega_{n+m-1} \qquad (10)$$

where an integral of $(n+m-1)$-order must be calculated. The rules to construct this integral are simple; each arrow on Figure 1 gives a multiplier (real or complex according to the diagram arrows), the last multiplier takes into account the signal detuning Ω_n and the accumulated spectral shift.

The SHG intensity at frequency $\omega \approx 2\omega_0$ for coherent laser pulses can be calculated using Equation (11)

$$S^{(\mathrm{SHG})}(\omega) \propto R(\omega)\left| \int \mathrm{d}\omega'\,\chi^{(2)}(\omega,\omega',\omega-\omega')\,E(\omega')\,E(\omega-\omega')\right|^2 \qquad (11)$$

where the $R(\omega)$ is a smooth spectral filter function of the SHG crystal and detection system.[109,110] $R(\omega)=1$ is a good approximation for pulses longer than 10 fs in duration and a thin SHG crystal; in this case the spectral power of SHG is proportional to the power of the second-order polarization. This polarization is proportional to the spectral amplitude introduced by the nonlinear effective field in Equation (12):

$$E^{(2)}(2\omega_0 + \Delta) = \int |E^2(t)|\,e^{i(2\varphi(t)+\Delta t)}\mathrm{d}t$$
$$= \int |E(\Omega)|\,|E(\Delta-\Omega)|\,e^{i(\varphi(\Omega)+\varphi(\Delta-\Omega))}\mathrm{d}\Omega \qquad (12)$$

where ω_0 is the carrier frequency of the pulse, Δ is a detuning value relative $2\omega_0$ and Ω is a detuning value relative Δ. In analogy to SHG, ISRS (see Figure 1) is a second-order nonlinear optical process. This effective electric field is proportional to the polarization given in Equation (13):

$$P^{(1-1)}(\omega) \propto \int \mathrm{d}\omega'\,\chi^{(2)}(\omega,\omega',\omega-\omega')\,E(\omega')\,E^*(\omega'-\omega) \qquad (13)$$

In the absence of an intermediate state resonance the spectrum of the effective field at a frequency $\Delta \approx 0$ is given by Equation (14):

$$E^{(1-1)}(\Delta) = \int |E(t)|^2\,e^{i\Delta t}\mathrm{d}t = \int |E(\Omega)|\,|E(\Omega-\Delta)|\,e^{i(\varphi(\Omega)-\varphi(\Omega-\Delta))}\mathrm{d}\Omega \qquad (14)$$

where Δ is a Raman frequency. This field does not depend on phase variations in the time domain $\phi(t)$ of the electric field.

The nonlinear signal is proportional to the integral of the nonlinear cross-section $\sigma^{(n)}$ times the absolute value square of the effective nonlinear field $|E^{(n)}(\omega)|^2$ over the frequencies [Eq. (15)]:

$$S^{(n)} \propto \int \sigma^{(n)}(\omega)\,|E^{(n)}(\omega)|^2\mathrm{d}\omega \qquad (15)$$

The nonlinear absorption does not depend on the phase of the nonlinear field $E^{(n)}(\omega)$; it only depends on the spectral power. The probability of multiphoton processes is given by Equation (16):

$$W = \sigma^{(n)}\,I^n\,\tau \qquad (16)$$

where I is the intensity of light and τ is the pulse duration. The weak-field approximation is correct below saturation, $W=1$. The experimental signature of the weak field regime is the polynomial (I^n) dependence of laser-induced emission. The two-photon cross-section can be quantitatively measured in units called Goppert–Mayer (GM) ($10^{-50}\,\mathrm{cm}^4\,\mathrm{s}$). The most common fluorescent dyes have two-photon cross-section values in the range 100 GM.[111] In the case of tight focusing (1 μm diameter) of 10 fs, 800 nm, 100 MHz saturation of two-photon transition appears at an average power of only 20 mW.

We illustrate in Figure 2 the multiphoton effects of phase modulation on 2PA at the detuned frequency $2\omega_0+\Delta$ and on ISRS at the frequency Δ, calculated in the frequency domain using the previously defined effective fields $E^{(2)}(\omega)$ and $E^{(1-1)}(\omega)$ [Eqs. (12) and (14)]. These effective fields are the result of multi-photon intrapulse interference (MII).[95,96,98–102,112] All three words in this definition are essential; it is the interference of the field with itself in the process of multiphoton transition. The spectrum of the pulse is very broad (for a 10 fs laser pulse, the FWHM is about 100 nm) and different parts of the pulse (photons with different frequencies) interfere with each other. For the 2PA example, photons with frequency $\omega_0+\Delta/2+\Omega$ combine with photons with frequency $\omega_0+\Delta/2-\Omega$ to cause absorption at frequency $2\omega_0+\Delta$ (see Figure 2c). Or, in the case of stimulated Raman transition, the pump photon at frequency $\omega_0+\Delta+\Omega$ combines with the Stokes photon with frequency $-(\omega_0+\Omega)$ (negative frequency because it is stimulated emission) to induce a transition at the wave number $\nu=\Delta/2\pi c$ (see Figure 2d). In this case, a photon with energy $+\Omega$ finds a counterpart with energy $-\Omega$, to give the two-photon stimulated Raman process. Mathematically speaking, the effective fields combine multiplicatively $E^{(n-m)} \propto E^n E^{*m}$. Because

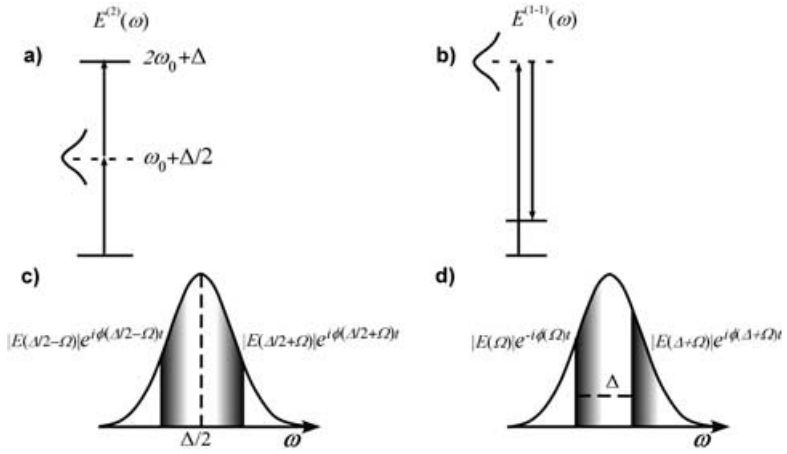

Figure 2. Multiphoton intrapulse interference for 2PA and for ISRS. The signal for 2PA results from absorbance of two photons as shown in (a). The signal for ISRS results from the action of two photons, one of them (Stokes) detuned by an amount Δ. Panel (c) illustrates the mirror image symmetry required by the phase function to enhance 2PA. Panel (d) illustrates the translated symmetry required by the phase function to enhance ISRS.

there are many different frequencies Ω in the spectrum these multiple pathways give "normal" interference in the sense of Brumer–Shapiro or Tannor–Rice definitions. This interference is accounted for additively or by integration over all possible Ω. There are two kinds of interferences in MII. The first is multiplicative interaction of the two photons (Ω and $-\Omega$), the second is additive averaging over all possible pathways Ω values. MII occurs whenever spectrally broad pulses induce multiphoton transitions.

To control multiphoton transitions, we can change the spectral phase of the pulse to control the intrapulse interference. We first make some important comments about the systems discussed in this Review. The systems have no intermediate resonances; so there is no interference between different resonant and nonresonant pathways. The strength of the electric field is not high, such that only a small number of photons are responsible for the nonlinear effects (2PA, 3PA, ISRS, CARS or photon echo). Under these conditions, one can prove using Parceval's theorem, that TL pulses ($\phi(\omega) \equiv 0$) maximize multiphoton transitions at all frequencies, but without any selectivity. The goal of controlling multiphoton transitions is to achieve the TL maximum probability at some frequencies and suppress the effect at different unwanted frequencies. This spectral selectivity of multiphoton effects is achieved by changing the spectral phase of the fundamental field.

3. Control of Spectral Narrowing in Multiphoton Processes

First, we address the suppression of two-photon excitation or SHG generation that is observed when the spectral phase of the laser pulse is not linear with respect to frequency. In particular, we systematically explore the best phase function to achieve SHG signal in a very narrow spectral window, while the intensity of SHG outside the desired window is suppressed. This is known as spectral narrowing. We chose this problem because it can be both calculated analytically and tested experimentally, it is useful for selective two-photon transitions, and it is a good model for the use of phase to suppress unwanted quantum mechanical transitions and to optimize a specific outcome.

We start by defining the goal and the parameters to be optimized using pure phase modulation of the fundamental pulse. In Figure 3a we show the spectrum of the effective field that induces SHG, namely $I^{(2)} = |E^{(2)}|^2$. One control parameter is the position of the maximum of the spectrum λ_m. The spectral detuning range (λ_{min} and λ_{max}) is the main control parameter. I_0 is the maximum of the spectral intensity. The spectral width can be defined for some level of intensity; the definition chosen depends on the general shape of the spectrum. For a smooth, bell-like shape, spectral width is usually defined as FWHM. For shapes that are more irregular, a definition such as level $x = 10\%$ is more useful. The integrated intensity inside this window is defined as the signal (S_x) and the integrated intensity outside this range can be defined as the background (B_x). This value is usually normalized using the total available intensity, that is, the integrated intensity for TL pulses. The performance is determined by the signal-to-background (SB_x) ratio. The degree spectral narrowing (SB_w) is characterized as a percentage compared to TL FWHM or to a fixed width w. For SHG or 2PA without intermediate resonances any phase modulation can only decrease the SHG intensity, hence TL pulses produce the strongest signal. However, TL pulses generate signal outside of the desired window (shown schematically in Figure 3). To achieve TL intensity inside the window while minimizing the signal elsewhere, we explore different phase functions.

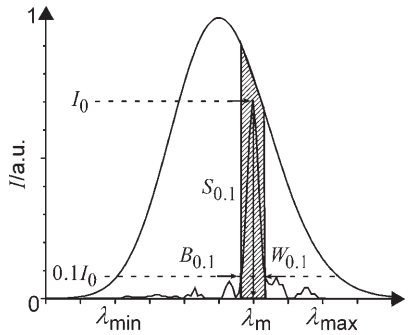

Figure 3. Schematic representation of the resulting SHG spectrum and parameters used to compare different approaches The Gaussian profile corresponds to the SHG spectrum of TL pulses. SHG narrowing is measured by defining as the signal S as integral in the region of width $W_{0.1}$ measured at the level 0.1 of the maxim I_0 centered at λ_m (hatched area). The background B is integral outside the dashed area.

3.1. Wavelength Tuning and Amplitude versus Phase-Shaping Modulation

The discussion of spectral narrowing is relevant only in the context of broad-bandwidth ultrashort pulses and multiphoton excitation. Long pulse and continuous wave (CW) lasers have extremely sharp bandwidths. For example, in Figure 4 we show the SHG spectra of a tunable 100 fs TL pulse scanned over the central frequency region from 700 to 900 nm. The SHG spectra are sharp and have a constant energy over the spectral region denoted by the dashed line, which corresponds to the bandwidth of a 10 fs laser pulse with the same energy as the 100 fs laser pulse. Tuning a laser requires re-optimization of the laser system and adjustment of other optics. Herein, we focus on the goal of achieving similar wavelength tuning by phase modulation of a very short pulse. Achieving wavelength tuning by phase modulation provides much greater flexibility in the creation of arbitrary nonlinear excitation spectra.

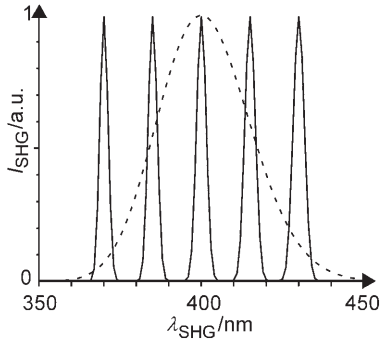

Figure 4. Selective SHG excitation resulting from frequency tuning of 100 fs laser pulses. The dashed Gaussian profile corresponds to the SHG spectrum of 10 fs pulses with the same energy in the fundamental pulse.

Ideally, one would want to have the high nonlinear conversion efficiencies of a shorter pulse and the flexibility of fast and easy tuning over a large bandwidth. Using 10 fs pulses, one could propose to achieve spectral narrowing by amplitude masking. The mask simply restricts the spectral window as shown in Figure 5a. As the window is scanned across the spectrum, a high contrast ratio can be achieved. Although amplitude masking works well (a good *SB* ratio), the amplitude of the obtained SHG is extremely small. This effect is shown in Figure 5, where three different amplitude windows are used to restrict the spectrum of the fundamental pulse, and the resulting SHG output spectrum is plotted. The observed decrease in SHG intensity caused by amplitude modulation implies that most frequencies inside a pulse contribute to the SHG signal. Because of the significant reduction in signal, we will not discuss amplitude modulation further. More importantly, we will show that similar spectral narrowing can be achieved by phase modulation without the significant loss of photons.

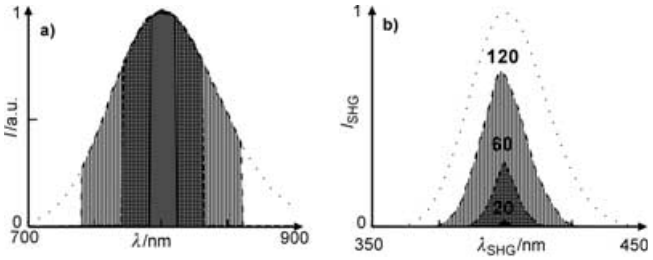

Figure 5. Evaluation of amplitude masking for selective SHG excitation. Three different amplitude masks were evaluated. a) The fundamental spectrum of the 10 fs pulse and the three amplitude masks with spectral windows of width 120, 60 and 20 nm. b) The resulting SHG spectra for TL pulses (black line) and for the corresponding windows given in (a). Notice the significant reduction in SHG intensity used by narrowing the amplitude mask.

3.2. Linear, Quadratic, and Cubic Phase Modulation

We begin our systematic study of phase shaping by analyzing the effect of phase masks with a simple functional dependence on frequency across the bandwidth of the fundamental laser pulse, and explore the effect of such phase modulation on the effective second-order electric field.[96] A linear phase function advances or delays a pulse in time, but it does not affect the resulting SHG output as shown in Figures 6a, 6d and 6g. Similarly, we see in Figures 6b, 6e and 6h that a quadratic phase modulation function broadens the pulse by advancing or delaying the higher frequencies (not shown explicitly) and can also advance or delay the pulse in time. The spectrum of the SHG output is not changed, but its amplitude decreases. The previous observations can be understood from the fact that the effect of phase modulation on two-photon processes can

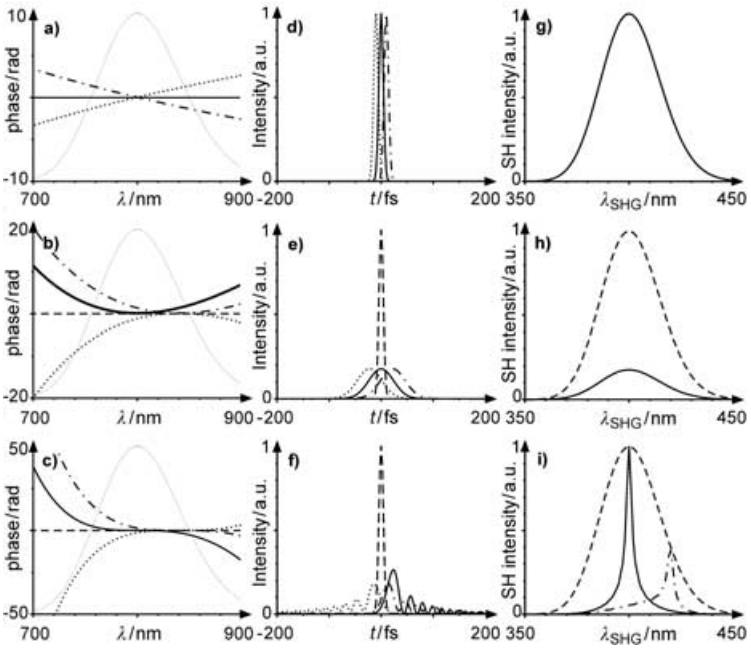

Figure 6. The effect of linear, quadratic and cubic phase modulation in the time and frequency domain including the SHG spectrum. Panels (a–c) show the fundamental spectra; panels (d–f) show the intensity as a function of time; panels (g–i) show the SHG spectra. In all panels the dashed lines are for TL pulses.

be considered to depend on the second derivative with respect to the frequency of the phase modulation. In fact, for a constant $\phi''(\omega)$ Equation (17) is valid:

$$I^{(2)}(\omega_0) = I^{(2)}_{TL}(\omega_0)\left(1 + (4\ln(2)\phi''(\omega_0)/\tau^2_{TL})^2\right)^{-0.5} \quad (17)$$

The second derivative of a linear function is zero, hence it has no effect on $I^{(2)}$. The second derivative of a quadratic function is a constant, and it always corresponds to a proportional decrease in the observed SHG output. Furthermore, because it is a constant, its effect on SHG does not depend on the frequency about which the quadratic dependence is centered, as can be seen in Figures 6b and 6h.

Cubic phase modulation has a significant effect on the SHG output because it has frequency-dependent nonconstant second derivative. In fact, a maximum is observed at the inflection point of the cubic phase function, where the second derivative is zero. Notice in Figure 6i, that the SHG spectrum resulting from cubic phase modulation is much narrower and is insensitive to the sign of the phase modulation. From this systematic analysis we note that spectral narrowing of a second-order process requires a phase function that has at least a third order dependence on frequency. Cubic phase modulation is good for spectral narrowing; however, technical implementation requires a phase shaper that is capable of very large phase retardation because of the cubic dependence on frequency may require retardations exceeding 100π at the extremes of the pulse bandwidth.[101] In conclusion, the ideal phase requires a nonconstant second derivative but does not diverge with increasing or decreasing frequency.

3.3. Sinusoidal Phase Modulation

From the previous discussion, it is clear that the sine function is a reasonably good choice for phase modulation. The Taylor expansion of the sine function contains cubic frequency dependence as one of its main parameters. The sine function has the advantage that it does not diverge towards infinity for higher or lower frequencies. The effect of sinusoidal phase modulation has been explored and an exact analytical formula for the spectral amplitude has been obtained.[82] Assuming a Gaussian power spectrum with FWHM corresponding to the TL pulse in the time domain τ_0, sinusoidal phase modulation with amplitude α, and spectral modulation frequency γ centered at ω_c the field is given by Equation (18):

$$E(\omega) \propto \exp\left[-\frac{(\omega-\omega_0)^2\tau_0^2}{8\ln 2}\right]\exp[i\alpha\sin(\gamma(\omega-\omega_c))] \quad (18)$$

This spectral shape corresponds to a train of pulses in the time domain, with temporal separation γ between adjacent pulse maxima [Eq. (19)]:

$$E(t) \propto \sum_{n=-\infty}^{\infty} J_n(\alpha)\exp\left[-\frac{(t-t_0-n\gamma)^2 2\ln 2}{\tau_0^2}\right]\exp[-in\gamma(\omega_c-\omega_0))] \quad (19)$$

where J_n is the Bessel function. The spectral amplitude of the second-order field is given by Equations (20) and (21)

$$E^{(2)}(\omega) \propto \exp\left[-\frac{(\omega-2\omega_0)^2\tau_0^2}{16\ln 2}\right]\sum_{n=-\infty}^{\infty} a_n \quad (20)$$

where

$$a_n = J_n\left(2\alpha\sin\left[\frac{1}{2}\gamma(\omega-2\omega_c)\right]\right)e^{in\pi/2}2^{-(n\gamma/\tau_0)^2} \quad (21)$$

In Figure 7 we show results calculated analytically [with Eq. (20)] and numerically [Eq. (12)] for a pulse centered at $\lambda_0 =$ 800 nm, $\tau_0 = 10$ fs, $\lambda_c = 2\pi c/\omega_c = 760$ nm and 780 nm, $\gamma = 10$ fs, $\alpha = \pi$. The maximum SHG is obtained at $0.5\lambda_c$ with some small systematic deviations caused by the spectral power not being

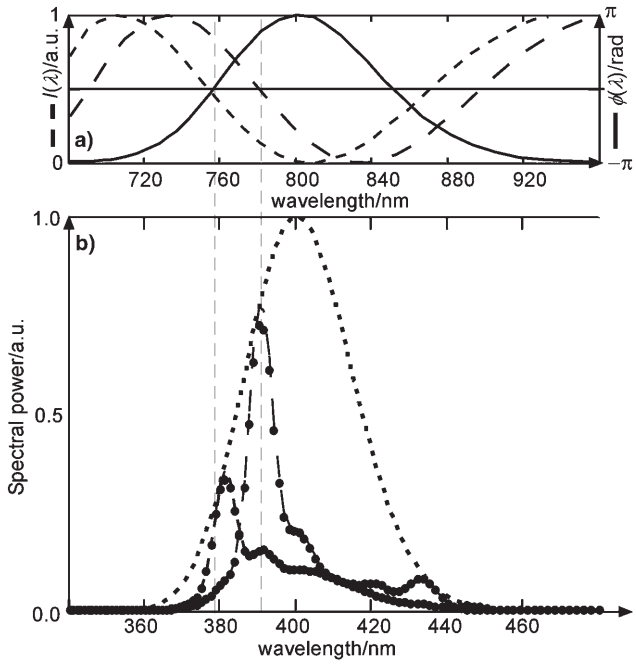

Figure 7. Effect of sinusoidal phase modulation on the SHG spectrum. a) Spectral power of the fundamental pulse (-----) and sinusoidal phases imposed on the pulse. b) Calculated SHG spectra for the TL pulse (•••••) and for the two phase functions shown in panel (a).

unity across the spectrum. The first term in Equation (20) is a good approximation for the maximum, but to calculate the whole spectrum we should keep the terms that satisfy the condition $n \geq \tau_0/\gamma$. Notice that the SHG intensity at $0.5\lambda_c$ reaches the TL value with a narrow spectrum. Unfortunately, as λ_c is tuned to the blue or red wings of the spectrum a significant background outside the wavelength of interest remains.

3.4. Using a Randomly Varying Phase to Suppress 2PA

For completeness, we explore another simple and intuitive method for achieving spectral narrowing in two-photon excitation. Here, we consider the construction of a phase function

that is flat in the region of interest and is random (each pixel varying in retardation value from 0 to 2π) elsewhere. The effect of random phase shaping for spectral narrowing is shown in Figure 8. The results reflect that this simple approach is quite successful in achieving narrow excitation; however, the amplitude achieved at the desired frequency is not very high, approximately 25% of the amplitude that can be achieved using TL pulses.

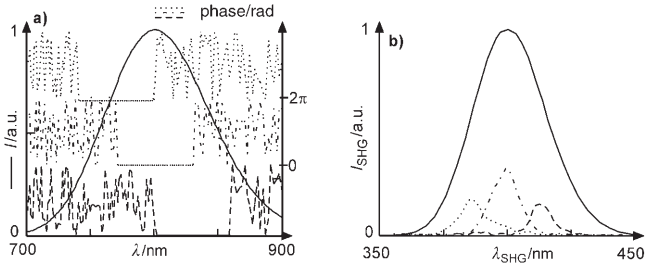

Figure 8. Control of the SHG spectrum using random phase modulation functions. a) Spectral power of the fundamental (——) and phase (•••••, ----- or –•–•) shown for different tuning values. b) Corresponding SHG spectra obtained from TL pulses and the corresponding SHG from phase-modulated pulses.

4. Binary Phase Shaping

The systematic analysis presented in Section 3 has allowed us to identify the sine function as very useful for phase modulation; however, an exhaustive search of all possible functions would take an impractical long time. Instead of such a search, we look carefully at Equations (12) and (14) to realize that for each frequency ω, one needs to integrate over a dummy variable Ω to determine the relative phase between photon pairs with upshifted and downshifted frequencies. The square of the sum of the phases from each different photon-pair combination, responsible for an amplitude at frequency ω, is maximized for full constructive interference but it can also be zero for complete destructive interference. By setting the phase values to 0 or π the contributions from each photon pair are restricted to 1 or -1, respectively. With these two values it is easy to design phases where the sum is maximized or zero. Binary phase functions are therefore the most efficient method we have found to achieve complete suppression of unwanted multiphoton excitation paths.[101] We have tested this hypothesis and have obtained outstanding results and efficiencies.

4.1. Fresnel-Inspired BPS

Based on the idea of binary phase shaping and Fresnel lenses, we set out to "focus" the SHG spectrum. In Figure 9 we present the results from this effort, where the binary phase function is given by Equation (22):

$$\phi(\omega_c,\omega) = \left|\pi \mathrm{round}\left[\frac{1}{2}\phi''(\omega-\omega_c)^2/2\pi\right]\right| \qquad (22)$$

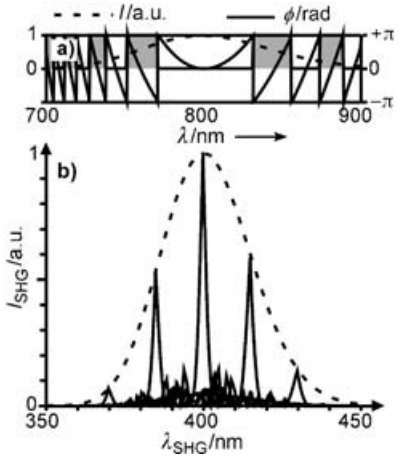

Figure 9. Control of the SHG spectrum using a Fresnel-inspired binary phase function. a) Fresnel phase modulation, green is the phase based on quadratic modulation. b) The resulting SHG spectra for TL pulses (-----) and for corresponding binary phase functions centered at different wavelengths.

where ϕ'' is the parameter that characterizes the parabolic focusing function and ω_c is the center of the SHG spectrum. For these examples we used $\phi'' = 8\tau_0^2$ and FWHM τ_0 of 10 fs. Remember that quadratic phase modulation has no narrowing effect on multiphoton processes (see Section 3.2). To focus the SHG, we replaced the continuous quadratic-wrapped phase with a binary phase by setting the phase equal to π when the Fresnel function is positive and 0 when it is negative (see Figure 9a). This function is symmetric $\phi(\omega_c+\Omega) = \phi(\omega_c-\Omega)$ at the center frequency ω_c. Notice that this BPS function reaches the TL value at the desired frequency because of its symmetry. We can see that the SHG output is sharp (FWHM is 2 nm) and tuning can be achieved over the relatively small range by translating the mask. The SB ratio is not very good (in the 1–2 range). Outside of the focusing region, the spectrum has a noiselike pattern near the value corresponding to the chirped pulse spectrum.

4.2. Prime-Number-Inspired BPS

There are three principles for constructing a binary phase to focus the second-order effective field at some frequency. First, the binary phase must be symmetric or antisymmetric about the focusing frequency to obtain TL amplitude at the center of symmetry. Second, to suppress the background, the phase function must have no other symmetry points; that is, it has to be pseudo-random. Any local symmetry will produce nonzero background. Third, around the focusing point, the phase must be constant.

Based on these three principles, we constructed a solution inspired by prime numbers. In this case, the phase switches from one value to another (0 or π) on every prime number counting from the edges, and blacking out the center eight pixel region of the 128 pixels defining the function. Shifting the entire phase function causes tuning of the narrow SHG peak. The gap generated at the edge upon tuning is filled by one pixel jumps in the phase. The results from the prime

number solution are shown in Figure 10. We can see that the results are slightly better than those obtained by the Fresnel-inspired solution.

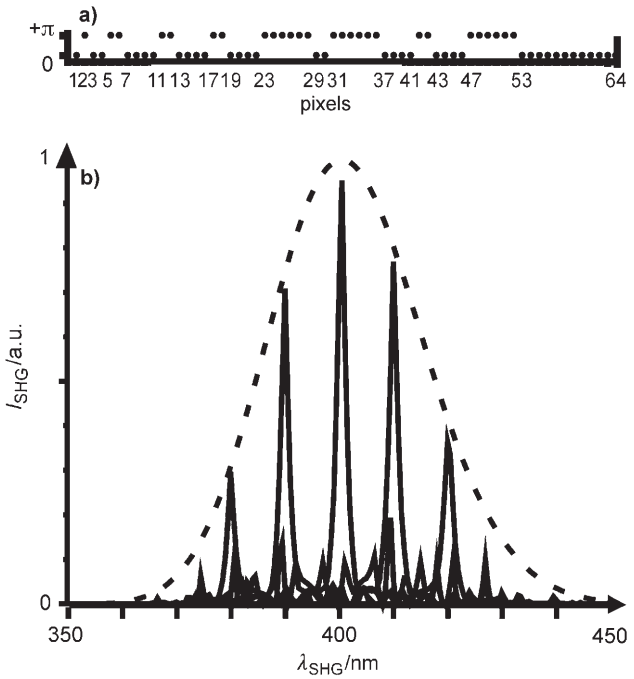

Figure 10. Control of the SHG spectrum with a prime-number-inspired binary phase function. First half of the prime-number-inspired phase function. The other half is obtained by mirror reflection. b) The resulting SHG spectra for TL pulses (dashed line) and for the binary phase functions centered at different wavelengths.

5. Evolutionary Learning Algorithms and BPS

As was shown in the previous section BPS can provide phase modulation to focus the SHG spectrum. The solutions we have given have some intuitive background. To improve the quality of the solutions, we have used an evolutionary learning algorithm, also known as a genetic algorithm, or GA, which is based on evolution towards a user-specified target. A flowchart of the GA is presented in Figure 11. The GA begins with a starting population, which is a list of strings of binary phases called genes. These genes, called individuals, can be randomly generated or constructed based on a priori knowledge of the problem. Each individual is evaluated experimentally (in the laboratory or via numerical calculation) and is assigned to a fitness value, which is a measure of how close an individual is to achieving the desired target. Individuals are then ranked according to their fitness. The lowest-ranked individuals ("losers") are discarded, while the higher-ranked individuals are used to construct the new generation of individuals, also known as "children". Children can be constructed from the list of parents using a variety of methods, including mutation, in which randomly selected genes or blocks of genes of a parent are either inverted or set to a single value, and crossover, in which two parents exchange a randomly chosen block of genes. The GA repeats the cycle of fitness evaluation, parent selection, and

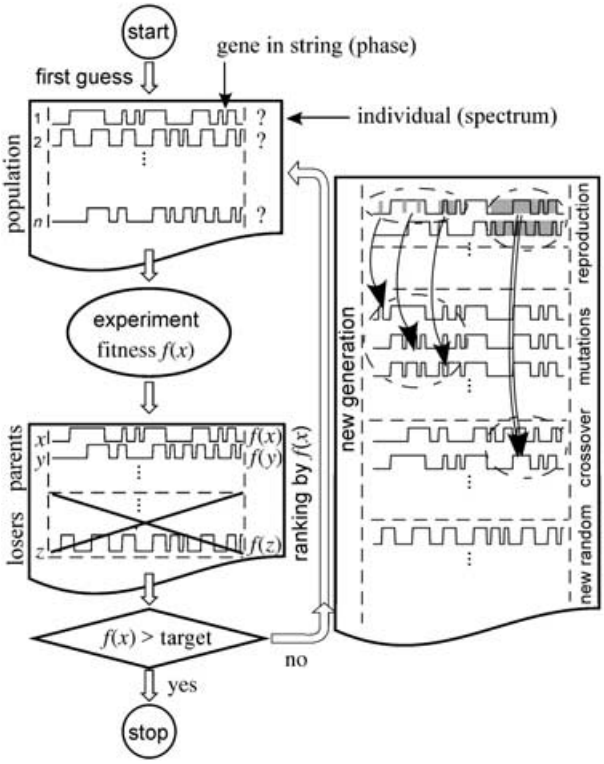

Figure 11. Typical flowchart for the genetic evolutionary learning algorithm used herein.

child generation many times until it either produces an individual with a fitness satisfactorily close to the target or fails to continue making progress.

Our GA used only mutation as the mechanism of child generation. The population consisted of 40 individuals with only one surviving parent. The first 10 children result from single-point mutations, the next 10 have a random number of mutations in random positions, and the rest of the population results from random block mutations. To reach good results we usually need to run this rudimentary GA for 50 to 200 generations. We used the GA to improve the previously found solutions for three distinct cases: focusing the SHG spectrum as sharp as possible without losing peak intensity, maximization of selective excitation on red or blue sides of the spectrum, and scanning a narrow SHG line across the widest possible spectral range without losing amplitude. The results of numerical experiments are discussed below.

5.1. Narrowing the SHG Output Using a GA to Optimize BPS Solutions

In the first experiment (Figure 12), the fitness function was defined as the ratio between the SHG focused within 1 nm of the center of the SHG spectrum over the SHG background outside the window ($SB_{1\,nm}$). As a first guess we used the prime number solution discussed earlier (Figure 12a); we mirrored mutations on both sides of the string of genes to preserve the symmetry required for two-photon excitation. The GA gave a very good improvement: the fitness $SB_{1\,nm}$ increased by a

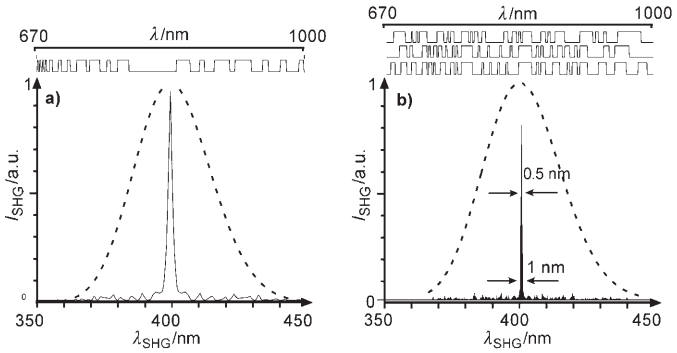

Figure 12. Spectral narrowing of the SHG spectrum using a) prime-number-inspired binary phase function and b) an improved binary phase function based on previous results using the GA. Three equally good solutions are given. The phase functions result in overlapping SHG spectra with slight difference in the background.

factor of three from 0.66 for the first guess to 2.0 for the GA solution. The FWHM of the resulting SHG spectrum is only 0.5 nm, which corresponds to a 0.5 pixel resolution in the fundamental spectrum. The amplitude of the SHG signal is close to the TL limit. Three results of GA runs are shown in Figure 12b. By running the GA program three times we obtained three solutions. It is interesting that there are no common patterns between these solutions (only their symmetry). There are probably many equally good solutions to this SHG narrowing problem. The background for these solutions is all different, but it is equally small.

5.2. Selective Excitation of a Chromophore Using BPS and a GA

Another important task solved using the GA is maximization of SHG in the red or blue side of the spectrum (see Figure 13). This type of phase modulation is important for selective two-photon excitation.[98,99] For this case, the fitness function was the ratio between the integrated SHG amplitude below 400 nm and that above 400 nm, and vice versa. The initial guess was zero modulation in the desired region and random phase (0 or π) for each pixel in the background region. Results

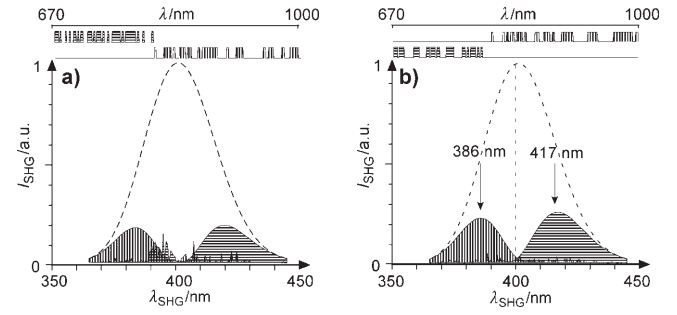

Figure 13. Generation of a broad SHG spectrum in the blue or red half of the available spectral range using (a) a random binary phase function or (b) an improved phase function using the GA. Notice the GA significantly reduced the undesired background.

from the initial guess are shown in Figure 13a. The GA improved on the random solution (see Figure 13b). SHG intensity in the desired band is increased significantly. The signal to background ratio $SB_{<400\,nm}$ or $SB_{>400}$ was 30. This means that the background was only 3% of the total SHG signal. This result is much better than for random, cubic or sinusoidal modulation, discussed earlier. This method has been used by us for achieving selective two-photon microscopy in condensed phase, when the broad 2PA spectrum has a spectral shift that is dependent on the chemical environment.[98] We have used this result to demonstrate functional imaging based on two-photon excitation through scattering biological tissue.[102,113]

5.3. Scanning the SHG Output Using BPS and a GA

The third task we have addressed is scanning a narrow SHG region in the broadest range possible. The initial guess was the Fresnel solution, presented first in Figure 9a and now in Figure 14a. Note that there is significant background when

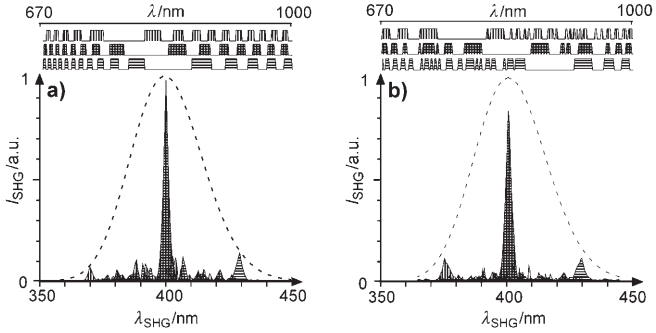

Figure 14. Generation of a narrow SHG spectra tuned across the available spectral range with a) Fresnel-inspired binary phase functions and, b) improved binary phase functions using a GA. Notice especially at the bluest and reddest wavelengths the increased intensity of the main peak and the decrease in the background.

trying to reach the limits of the tuning range for this method. Using the GA we achieved much better results, especially when this method is pushed to the limits of the spectrum. In those cases, the GA achieved focusing 50% of the SHG within a 5 nm width while the rest of the energy is spread over the 80 nm background. A much cleaner situation was found when the sharp SHG feature was in the center. These tuning results are presented in Figure 14b. The range of tuning for the 10 fs initial TL pulse is close to the theoretical limit of 375–430 nm (55 nm). Note that this tuning range is achieved through phase modulation only; the fundamental beam is otherwise unchanged. Using a shorter initial TL pulse, say 5 fs, would increase the range of tuning beyond 100 nm. The ability to scan a narrow excitation region, as shown in Figure 14b, could be used for measuring multiphoton-excitation spectra with a resolution of a few nanometers in the range of several tens of nanometers.

6. Systematic Analysis of GA Solutions Using BPS

There are two reasons why the GA approach was introduced and still holds the greatest promise in the field of coherent control of chemical reactions. First, the Hamiltonian, which contains the required information about the system to predict its linear and nonlinear interactions with the electric field, is not known for most problems. Second, the field can be phase- and amplitude-modulated to produce from 10^{100} to 10^{1000} differently shaped pulses, making direct sampling of the whole space in search for the optimum solution impossible. GAs, commonly used for engineering applications, had the best potential to explore these immense search spaces.

If we are going to optimize multiphoton processes using a GA, it would be very important to know something about the structure of the search space. The first type of information we want to find out is the nature of the search space. At the extreme of simplicity, we would like to know if the search space is *convex*—where there is one clear maximum and the gradient always points toward the maximum (see Figure 15a). For a convex search space a steepest descent search, also known as a hill climber, is the most efficient method. A GA would also have a good chance of converging on the best solution if this solution were close to other relatively good solutions and were not an isolated point. At the extreme of complexity, the search space would resemble looking for a *needle in a haystack*. For this situation, the landscape is rough and contains a single isolated optimum solution, as shown in Figure 15b. For this case, random sampling has the same chances of finding a solution as a GA. Recently, Rabitz et al. published an article where they discuss the landscape of search spaces associated with coherent control of quantum mechanical systems.[114] They found that multiple solutions usually exist, and that all solutions are excellent solutions.

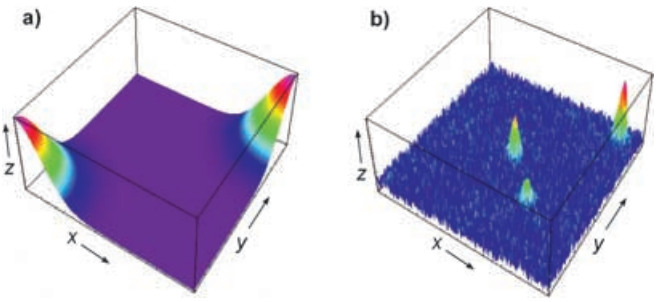

Figure 15. Schematic representation of the search space in a GA experiment. a) Representation of a convex problem, b) representation of a needle-in-the-haystack problem. *x* and *y* are two parameters used to label the different phase functions and *z* is the fitness.

Although there are some general discussions regarding the nature of the search space of coherent control problems,[114] there has been a problem to conceive and to represent a multidimensional space of the necessary magnitude. The root for this difficulty is that in the most general case, there are *N* pixels that can take *A* different amplitude values and *P* different phase values; resulting in a search space of size $(A \times P)^N$. If we decide not to use amplitude modulation on the basis that would be counterproductive to eliminate (throw-away) photons, the search space immediately reduces to P^N. However, in most cases this is still a prohibitively large number, except when one allows only phases of 0 and π, reducing the search space to 2^N a number that is hundreds of orders of magnitude smaller.[101]

6.1. Advantages of BPS Compared to Arbitrary Phase-Shaping Methods

Arbitrary phase modulation contains a great amount of redundancy evenly distributed between good solutions. As discussed in Section 4, we imagine that most of this redundancy arises from two properties of the electric field. First, it has a 2π periodicity. Second, nonlinear processes are affected only by the second and higher derivatives of the spectral phase. Therefore, the addition of a constant phase or a linear phase of any amplitude across the spectrum makes no difference. The use of BPS allows us to drastically reduce the search space without discarding all optimum solutions. The search space for the problem described above, using BPS, is of size 2^N. If we considered a 100 pixel shaper, the search space would be of size 10^{30}. If we use 32 pixels to optimize any two-photon excitation process, then there are only $\sim 10^5$ possible phase shapes. Symmetry allows us to modify only 16 pixels and assume the other 16 are mirror images of the first. This greatly reduced search space allowing mathematical calculations of all the solutions for a particular problem, and plotting of the entire search space for visual analysis and classification. In the following section, we explore the search space for a number of important pulse-shaping cases. The search space is presented by plotting the fitness of a particular binary phase as a function of *x*, and *y*, where *x* and *y* are decimal equivalents to the binary number represented by the first and second half of the binary string, respectively ($x = 1 + b_1 + b_2 2 + \ldots + b_8 2^7$, $y = 1 + b_9 + b_{10} 2 + \ldots + b_{16} 2^7$). This provides a map of the search space; note that phases such as 0111111 and 1000000, which appear very different in binary representation, have adjacent decimal equivalents.

6.2. Analysis of Specific Cases

6.2.1. Generating TL Pulses

In principle, maximum SHG generation is obtained for TL pulses. The problem of obtaining TL pulses by reducing unwanted phase distortions is known to be convex. Because SHG is only affected by phase functions having a nonvanishing second derivative [see Eq. (17)], there is a great amount of redundancy associated with this problem. Furthermore, small phase changes in the wings of the pulse make only very small changes in the measured output. Given the redundancies and the insensitivity of the method to small changes in the phase, the number of good solutions that are close to TL is extremely

large. It has been found that a priori knowledge of the result can be very valuable for speeding the GA's convergence toward the optimum solution. For example, it has been pointed out that smoothing, when introduced as a GA operator, helps the algorithm converge toward TL pulses. Unfortunately, in the more interesting cases of coherent control not enough is known about the solution to design simple operators that can be used to help the GA.

Here, we look at the problem of TL pulse generation from the point of view of BPS. The solution, having the maximum fitness, is known in this case and corresponds to TL pulses. We calculated the fitness for all possible 16-bit sequences used to produce symmetric 32-bit sequences. The binning of pixels is such that approximately each of the 16 pixels represents an equivalent amount of spectral amplitude taking into account the Gaussian spectral shape of the pulse (see Figure 16a). The numerically calculated search space (see Figure 16b) shows the nature of the search space to be convex, with solutions at the corners corresponding to TL pulses. Notice that there are discrete steps which correspond to binary switching of one and two pixels on pulses that are nearly TL. The GA sometimes converged on phases that were within one or two pixels of TL. The reason is that there is a much greater number of good solutions and any two optimum values are presented at the corners of Figure 16b. We believe that this situation is a reasonable illustration of a case in which the GA searches among arbitrary phases. In a later section we present an alternative method for using a pulse shaper to obtain TL pulses accurately and reproducibly.

6.2.2. SHG Spectral Narrowing

We have numerically calculated the entire search space for spectral narrowing as discussed in Sections 4 and 5. The results are shown in Figure 16c. The *z* axis corresponds to the ratio of the signal at the specified frequency divided by the integrated background outside the desired window. Notice that there are several optimum solutions, and that the majority of the phases are bad solutions. This problem is close to being a needle-in-a-haystack problem. In a later section we will discuss the evolution of a GA toward solutions of this problem.

6.2.3. Controlling Two- versus Three-Photon Excitation

We explored how phase modulation of the fundamental pulse can be used to maximize or minimize the ratio between two- and three-photon excitation. In the past, we have addressed this problem using a combination of sine and quadratic phase modulation.[95,96] Here, as before, we used 16 bits to encode a symmetric sequence of 32 pixels. We explored all possible combinations of binary phases and calculated, integrated and normalized second harmonic $I^{(2)}$ and third harmonic $I^{(3)}$ spectra. Not surprisingly, it is clear from these results that the maximum ratio of $I^{(3)}/I^{(2)}$ is achieved for TL pulses. The search space for this problem shown in the Figure 17 is convex and resembles that for optimization of SHG.

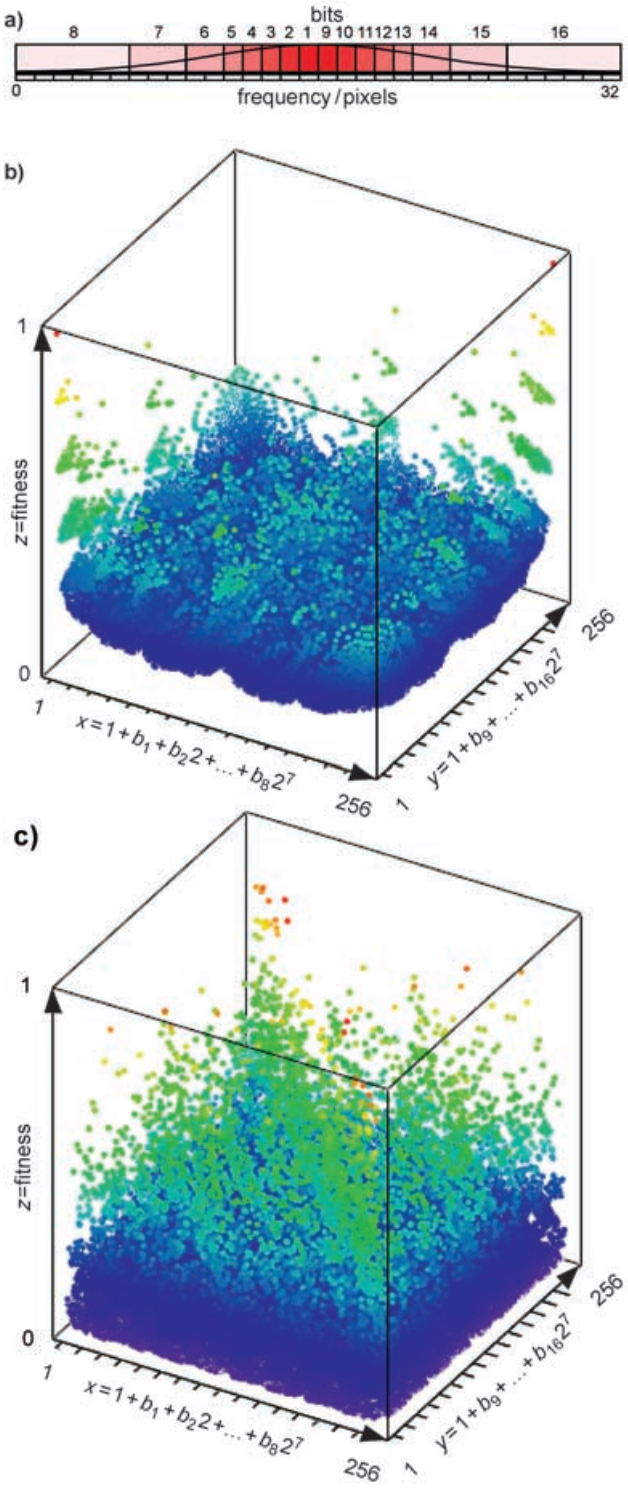

Figure 16. Three-dimensional representation of b) TL pulses and c) spectral SHG narrowing. a) Configuration of the Gaussian intensity weighted phase mask used to generate binary phase functions.

A more interesting problem is the optimization of the $I^{(2)}/I^{(3)}$ ratio, especially because it may be useful for biomedical applications where damage to healthy tissue by three-photon excitation of DNA needs to be minimized. For this case, shown in Figure 18, there are many equally good solutions. Any phase

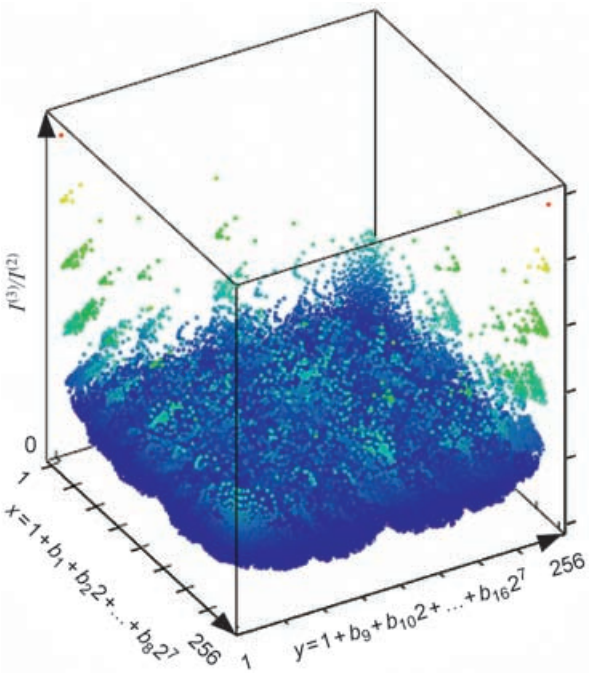

Figure 17. Three-dimensional representation of the search space for optimization of the integrated three- over two-photon excitation using 16-bit binary phase functions. Notice that the search space is identical to the search space for finding TL pulses in Figure 16b.

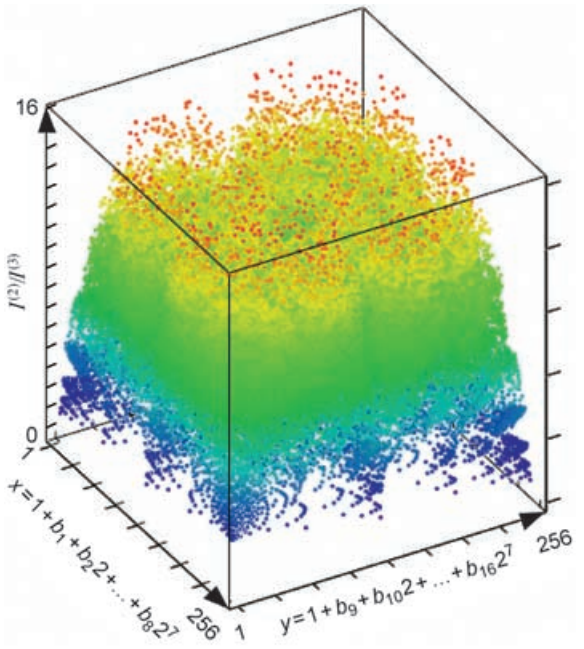

Figure 18. Three-dimensional representation of the search space for optimization of the integrated two- over three-photon excitation.

distortion lengthens the pulse and hence suppresses $I^{(3)}$ more than $I^{(2)}$. Phase distortion appears not to have particular regularities; all the good solutions are unrelated. In this case phase complexity efficiently lengthens the pulse. The time duration of the spectrally shaped pulse is approximately 16 times longer than the TL pulse. The ratio $I^{(2)}/I^{(3)}$ reaches this value for many of the possible phases, but there are still many more bad solutions than good ones (see Figure 18). The search space looks like "grass" with solutions on the top and a background of multiple bad solutions.

The next task we explored involved optimization of the $S^{(2)}/I^{(3)}$ ratio, the case in which second-order excitation takes place not on the whole spectrum ($I^{(2)}$), but in some limited spectral range (Δ) around the SHG maximum ($S^{(2)}$). This situation is a model for two-photon induced photodynamic therapy (PDT) using spectrally broad pulses and a therapy agent with a relatively narrow 2PA. The goal is to maximize the second-order process in some spectral range and minimize three-photon damage. In Figure 19 we show the best solutions for three

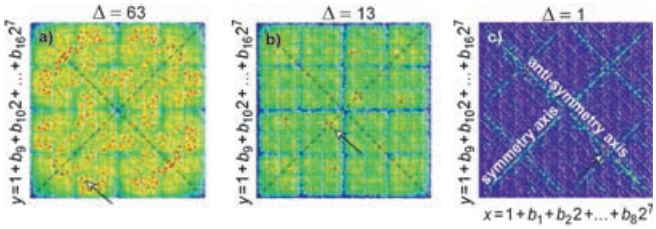

Figure 19. Two-dimensional representation of the search space for control of selective two-photon excitation $S^{(2)}$ versus integrated three-photon excitation $I^{(3)}$ for 16-bit binary phase function. a) Represents the case where $S^{(2)}$ excitation occurs over the whole spectral range. b) Represents the case where $S^{(2)}$ excitation takes place over a narrowed window. c) Represent case where $S^{(2)}$ excitation takes place over a very narrow spectral window.

cases: 1) the spectral window of excitation spans the whole width of the pulse, 2) it spans an intermediate width, and finally, 3) it has a very narrow width. For the broad window, we have many solutions: see the large number of red dots in Figure 19a. For the intermediate window there are several solutions (see Figure 19b), and for a narrow window there are fewer solutions (Figure 19c). In these cases suppression of the three-photon-induced damage of two orders of magnitude.

Interestingly, we can find some symmetry in the search spaces shown in Figure 19. There are two axes of symmetry; the phases are symmetric with respect to reflection around the axis ($y=x$) and antisymmetric around the axis ($y=2^8-x$). The best solutions for the narrow window are *anti*-symmetric. In Figure 20, we plot the fitness $S^{(2)}S^{(2)}/I^{(2)}I^{(3)}$ obtained after optimization using a GA for narrow SHG excitation for different window width. We choose this ratio for optimization for several reasons. By maximizing this ratio, we maximize two-photon absorption in some spectral window and minimize both integrated two- and three-photon absorptions. This ratio is dimensionless and has the limit $I^{(2)}/I^{(3)}$ for a broad window when $S^{(2)}\rightarrow I^{(2)}$. As seen in Figure 20 for broad windows, all points reach the theoretical limit ≈ 16; this value depends on the relative width of the pixel in the phase modulator. Phase modulation effectively broadens the pulse which becomes less effective at generating the third harmonic. The average duration of the pulse is approximately equal to $\tau_0 N$ where N is number of pixels inside the FWHM of the fundamental spectra. A similar

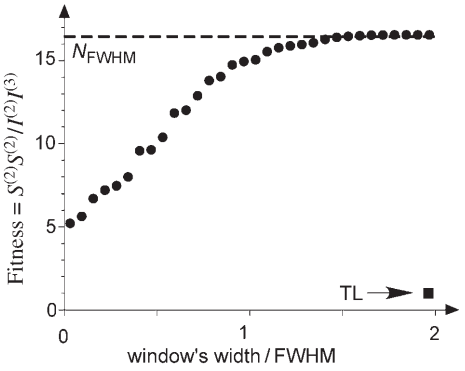

Figure 20. Optimum selective two-photon $S^{(2)}$ excitation over integrated three-photon excitation $I^{(3)}$ as a function of the width of spectral window. The optimum fitness value calculated for each spectral window is shown as a dot. In the data we see that as the window becomes narrow compared to the number of pixels of the phase function, the fitness value decreases. Suppression of $I^{(3)}$ is limited by the number of pixels in the shaper N_{FWHM}. The fitness value is normalized such that it equals one for a TL pulse.

effect will appear for lengthening of a TL pulse, but in our case, phase modulation allows us to control not only the amplitude but also the frequency at which multiphoton excitation takes place. We can focus two-photon excitation on the desired region and defocus three-photon excitation out of dangerous spectral regions.

Experimentally, we have shown that it is possible to suppress three-photon excitation while maintaining two-photon excitation at a relatively high level.[96] When the laser intensity is sufficient to cause third-order processes such as three-photon excitation efficiently, other third-order phenomena such as self-focusing take place. Under those circumstances, the effect achieved by phase modulation is amplified, and the control level enhanced.

We have used BPS to find the best solutions which focus the SHG spectrum at $2\omega_0$ while minimizing three-photon excitation at $3\omega_0$. The results are shown in Figure 21. The fundamental spectrum centered at ω_0 is focused on a narrow peak centered at $2\omega_0$ with a very small background. Two antisymmetric solutions, one optimized to suppress the integrated three-photon intensity and the other to minimize the signal at $3\omega_0$, are shown in Figures 21 a and 21 b, respectively. The integrated signal at $3\omega_0$ is suppressed by a factor of 600. Note that in Figure 21 b there is a hole at $3\omega_0$; clearly, complete suppression at $3\omega_0$ is possible. If we optimize the ratio between $I^{(2)}$ and $I^{(3)}$ in the center, then $I^{(2)}$ reaches the TL level and $I^{(3)}$ at $3\omega_0$ is suppressed at least by a factor of 2^{16}.

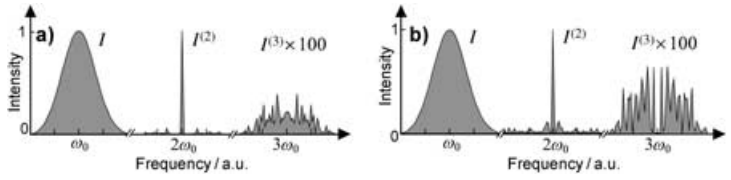

Figure 21. Control of a sharp two-photon excitation $S^{(2)}$ versus the integrated three-photon excitation $I^{(3)}$. The intensity of the fundamental field, the narrowed second harmonic and the third order intensity are plotted. Two cases are shown: in case (a) the integrated third harmonic signal was minimized; for case (b) the signal at $3\omega_0$ was minimized. Notice that in case (b) there is a hole at $3\omega_0$.

6.2.4. Selective Impulsive Stimulated Raman Scattering

The spectral power of ISRS can be presented as the Fourier image of the intensity of the shaped pulse in the time domain [Eq. (14)]. We begin our analysis by calculating all possible binary phase combinations and their effect on ISRS using 16 pixels, assuming the field to have a constant power across the spectrum. We calculated the frequency where ISRS is enhanced for all possible phase combinations (2^{16} possibilities) and used the ratio of spectral power at a specific (desired) Raman frequency $I(\Delta)$ to the full intensity of Raman scattering as the fitness function z. Figures 22 b–22 f (the left side panel) present the color-coded 2D plot of the search space. The best solutions are marked with a red circle; the corresponding stimulated Raman spectrum is represented on the right side panel. The upper part is the spectral amplitude of the shaped field $E(\omega)$ and the lower part is the Raman spectral power $I^{(1-1)}(\omega)$. The phase modulation is used to focus the stimulated Raman transition on a specific frequency. Notice that solutions where the stimulated transition is focused on the frequency corresponding to pixels 6 through 10 have a specific symmetry, reflected by the attraction of the solutions to the lines in the search space representation. For example, in panel (b) this is translated symmetry ($x=y$) and translated inverted symmetry ($y=2^8-x$). The translated inverted solution is always better than the translated symmetric solution, because for translated inverted symmetric sub-harmonics at half of the frequency of the maximum in the Raman spectrum are better suppressed. For the cases when the Raman spectrum is maximized away from the center of the spectrum, there are lines in the search space where the solutions are concentrated. These lines correspond to phases $\phi(\Omega+\Delta/2)-\phi(\Omega-\Delta/2)=0$ or π, where Δ is the maximum of the frequency of Raman transition. The reason why this symmetry provides the maximum Raman transition can be understood by analyzing Equation (14).

The case of translated symmetry $\phi(\Omega+\Delta)-\phi(\Omega)=0$ was discussed for periodic spectral modulation used to enhance CARS.[88,89,115] The case of translated inverted symmetry $\phi(\Omega+\Delta)-\phi(\Omega)=\pi$ is specific for BPS. As we found earlier, the translated inverted symmetric solution gives the same maximum at Δ as the translated symmetric case, but suppression outside the Raman frequency is better. To improve the quality of background suppression, we calculated the fitness function $z(x,y)=(I(\Delta)/(S-I(0)-I(\Delta))$ for all phases with this symmetry (translated and translated inverted); the plot of the fitness function is shown in Figures 23 b, 23 f and 23 j. When the maximum Raman transition is greater than half of the spectral width ($16=32/2$ in our case), we fill pixels in the central region of the spectrum, which cannot be shifted with zeros (see Figure 23 h). In both cases these methods achieve TL amplitude at frequency Δ and substantial suppression of the background. There are many good solutions; all of them are represented from red

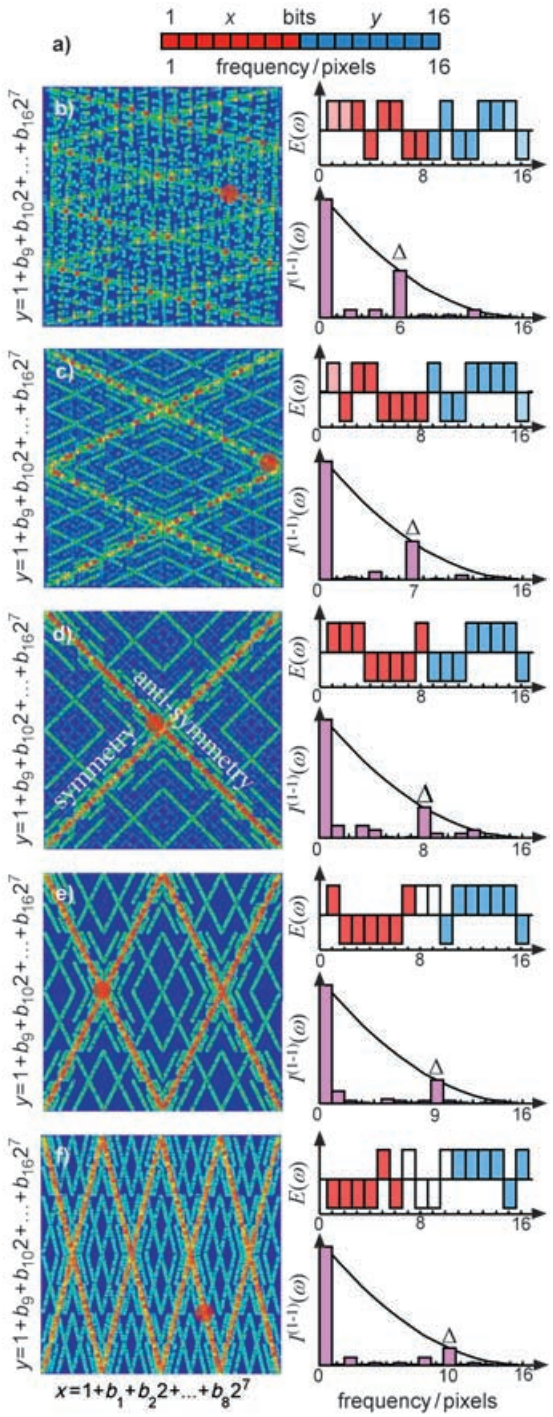

Figure 22. Selective ISRS control using binary phase functions. a) The 16-bit binary phase functions are divided into two regions, red and blue. The search space for each detuning value is presented on the left, while the best solution marked by a red dot is shown on the panels on the right together with the calculated spectrum.

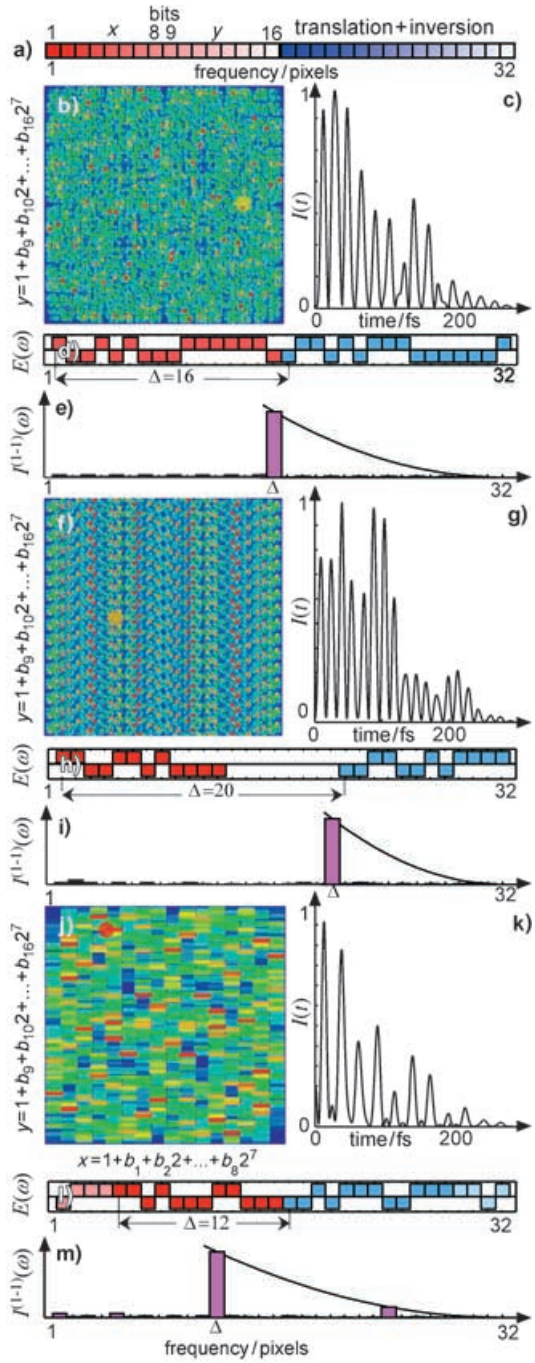

Figure 23. Selective ISRS control using a 32-bit binary phase function. a) The binary phase functions have translated inverted symmetry (16 bits encode 32 pixels). The calculated search space plots the fitness signal signal/background as function of phase for a given value of detuning Δ. The time-dependent field intensity is given for each case (c,g and k) for the best phases marked with a circle. For each case we show the best binary phase function and the resulting Raman spectra focused at the selected positions.

to yellow in the search space (Figures 23 b, 23 f and 23 j). The best solutions are plotted on the central panels. We can see that BPS achieves high selectivity for stimulated Raman transitions. In Figures 23 c, 23 g and 23 k, we show the calculated intensity of the laser pulse in the time domain for each of the solutions. We can see that the main period of field intensity oscillations corresponds to the Raman frequency. One could argue that complicated phase modulation is not necessary if amplitude modulation could generate two sharp lines with a frequency difference Δ to induce beats with the desired frequency. For stimulated Raman transitions such amplitude modulation would provide selectivity, but the intensity of the

signal would drop proportional to the square of the spectral width of the window. The signal would be lost as the spectral resolution is increased. This is similar to the case of amplitude modulation for two-photon excitation analyzed in Section 3.1.

6.3. Reduction of the BPS Optimization Task to Number Theory

We can formulate the problem of sharp focusing of two-photon transitions (such as SHG or ISRS) using a purely mathematical language, the advantage being that one is then able to distinguish properties that simplify computation considerably. First, we note that each spectral component of the electric field, linearly dispersed in the frequency domain, can be represented as a binary value (± 1) determined in Equation (23):

$$b_\Omega = \exp[i\,\phi_\Omega],\ \Omega = -m,\ldots,-1,0,1,\ldots,m \tag{23}$$

where $\phi = 0$ or π, respectively. For symmetry purposes we set the number of frequencies, Ω (pixels in SLM), to be an odd number $N_{odd} = 2m+1$, each at a position proportional to the frequency detuning from the carrier frequency ω_0 (linear scaling on SLM).

The spectral amplitudes of the electric field $A^{(2)}(\Delta)$ or $A^{(1-1)}(\Delta)$ are measured at the detuned frequency 2Δ from $2\omega_0$ or zero, respectively. If we assume that the amplitude of the electric field is constant, that is, we set the spectral power equal to 1 in the allowed spectral region, then nonlinear fields can be easily calculated. $A^{(2)}(\Delta)$ and $A^{(1-1)}(\Delta)$ are vectors with the same length N_{odd} and can be can be calculated with Equations (24) and (25):

$$E^{(2)}(\Delta) = a_\Delta^{(2)} = \sum_{\Omega=0}^{m-|\Delta/2|} b_{\Delta/2+\Omega} b_{\Delta/2-\Omega}$$
$$\Delta = -2m, \ldots, -2, 0, 2, \ldots, 2m \tag{24}$$

$$E^{(1-1)}(\Delta) = a_\Delta^{(1-1)} = \sum_{\Omega=|\Delta/2|-m}^{m-|\Delta/2|} b_{\Delta/2+\Omega} b^*_{-\Delta/2+\Omega}$$
$$\Delta = 0, 2, \ldots, 2m \tag{25}$$

The ISRS case gives a symmetric Equation (25) and we can analyze only positive detuning.

The problem of phase shaping effects on the nonlinear optical response can now be formulated as finding the vector b for any vector a to solve Equations (24) or (25). For the SHG process at $\Delta = 0$ and for the ISRS process at $\Delta = m$ Equations (24) and (25) can be further simplified as shown in Equations (26) and (27):

$$E^{(2)}(0) = a_0^{(2)} = \sum_{\Omega=0}^{m} b_\Omega b_{-\Omega} \tag{26}$$

and

$$E^{(1-1)}(m) = a_m^{(1-1)} = \sum_{\Omega=0}^{m} b_\Omega b^*_{\Omega-m} \tag{27}$$

Note that Equations (26) and (27) have multiple solutions [Eqs. (28) and (29)]:

$$\max E^{(2)}(0) = \max a_0^{(2)} = \pm(m+1) \ \text{ if } \ b_{-\Omega} = \pm b_\Omega \tag{28}$$

$$\max E^{(1-1)}(m) = \max a_m^{(1-1)} = \pm(m+1) \ \text{ if } \ b_{\Omega-m} = \pm b_\Omega \tag{29}$$

The condition for maximization of SHG is reflection symmetry around zero. To maximize ISRS, the second half of the spectral phase must be equal or opposite to the first half. From Equation (24) (for SHG) the condition requires symmetry of the phase about Δ. From Equation (25) (ISRS) the condition requires translation symmetry about Δ. The phases with these symmetry properties will give the optimum solutions.

Selective multiphoton excitation mathematically implies finding a vector b such that a is maximized for some particular Δ and is minimized at all other indices. This task belongs to the branch of mathematics focused on finding binary vectors with low correlations, typically used for secure communications. In the case of continuous bell-shaped functions, autocorrelation results in a continuous function with a width greater than the function itself. For discrete binary functions, autocorrelation can result in a delta function. This tells us that the spectral phase must be maximally symmetric with respect to a point of reflection (as in SHG) or some specific translation (as in ISRS) but maximally asymmetric with respect to all other points or translations. Pseudo-noise[116] or pseudo-random[117] sequences can give us some estimation of the level of background to be expected for selective multiphoton excitation. The merit factor for correlation (mean square dispersion of amplitude) for long sequences is approximately 10.[118] From our estimations the merit factor for convolution has the same magnitude.

We can estimate the magnitude of the signal to background ratio. From symmetry considerations, the signal at the selected frequency is proportional to m. The upper bound of the background amplitude for sequences with low aperiodic cross-correlations, is proportional to $m^{0.5}$.[119] These mathematical findings, from a physical point of view, imply that we can reach the TL limit in a narrow spectral region W/N (where W is the full spectral width and N is the number of pixels in the pulse shaper). The integrated intensity of the background is approximately proportional to 10% of the integrated intensity of the peak ($0.1 \times I_{TL}$) for any number of pixels. The background is suppressed and the integrated intensity of the background is bound by a value proportional to I_{TL}/N. Obviously using an SLM with more pixels provides better selective multiphoton control.

The solution of Equations (24) and (25) for any given function is the reverse task of finding a binary function knowing its convolution or correlation function. A precise analytical solution probably exists. For the long sequences when an exhaus-

tive search of all possible combinations is impossible we analyzed these tasks using evolutionary learning algorithms. All the successfully solved examples give hope that BPS is an extremely powerful method for controlling multiphoton interactions. The statistical properties of pseudorandom sequences is a subject of Number Theory which has many applications in science and technology.[120,121]

6.4. Analysis of the Search Space

We used a GA to search for an optimal binary phase for three specific problems: maximum SHG conversion, selective 2PA, and ISRS. It is very important to construct a proper fitness function for each task. If we want to suppress the background, we can choose a fitness function that rewards minimization of the integrated background intensity or of the mean square of the background. We choose to minimize the mean square of the background, because in this case we generate maximally flat multiphoton spectra without spikes. Maximization of total SHG has the obvious solution, namely, TL pulses.

Our tasks are similar to the task of finding the binary sequence having a minimum autocorrelation, a case that has been analyzed using evolutionary search.[122] Because there is always one symmetry for our examples, the size of the search space is $N_s = 2^{N/2}$. For a pulse shaper with $N = 32$ pixels, $N_s = 2^{16} = 65\,536$. It is possible to do an exhaustive evaluation of all possible phase combinations for a search space of this size. For a pulse shaper with $N = 64$ pixels, the search space is $N_s = 2^{32} \approx 4 \times 10^9$, making exhaustive evaluation of the search space impractical. Therefore, we use a GA to find the optimal solution in these large search spaces.

For simplification, we analyze BPS theoretically assuming a constant intensity across the spectrum of the pulses. To calculate SHG and ISRS spectra we use the fast Fourier transform (FFT) method.[123] To resolve aliasing problems when we calculated discrete inverse FFT of the square (SHG) or the absolute value of the square (ISRS) we padded N zeros in the right side of the fundamental spectrum. For a pulse shaper with N pixels the calculated spectra have $n = 2N-1$ points. Because the ISRS spectrum is the Fourier image of the intensity of the pulse in the time domain, the ISRS spectrum is always symmetric and we plot only the positive part (N points). The SHG spectrum in general is not symmetric around the center and we plot all $2N-1$ points. We normalize the intensity so that a TL pulse (in the center of SHG and at zero frequency for ISRS spectra) achieves unity. The shape of the spectrum generated by the TL pulse is more triangular than bell-shaped because of the flat top spectrum used.

First we analyze the results obtained from the exhaustive calculation of all possible results for ($N = 32$ bits). Because for BPS we have an additional symmetry that corresponds to interchanging 0 and 1 the size of the search space is $2^{N/2-1}$. The 64 best phase combinations, with maximum fitness are presented as 2D black and white plots in panels (a) in Figures 24–26 for maximum integrated SHG, selective two-photon excitation and ISRS, respectively. The fitness calculated for these individuals is presented in panel (b) in Figures 24–26 along with a dashed line corresponding to the theoretical limit. The spectral intensity achieved for the best result (from exhaustive calculation) is shown on panels (c) of Figures 24–26. Maximization of total SHG obviously requires a TL pulse. For selective 2PA and ISRS the best results are with mirror or translational symmetry, respectively.

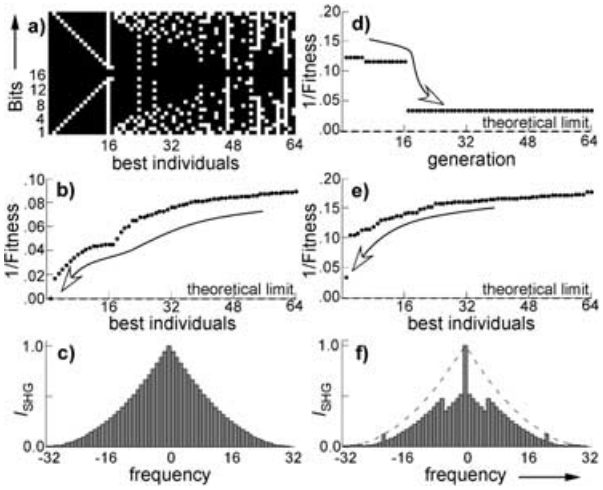

Figure 24. Exhaustive calculation and GA search for the phase that provides maximum integrated of SHG using 32-bit phase functions. a) The 64 best individuals from the full set of calculated phases sorted by fitness, b) the fitness of the 64 best phases, c) the global optimum solutions for this problem, d) progress of the GA, e) fitness of 64 solutions found during the last GA generation, f) the best SHG spectrum produced by the GA search.

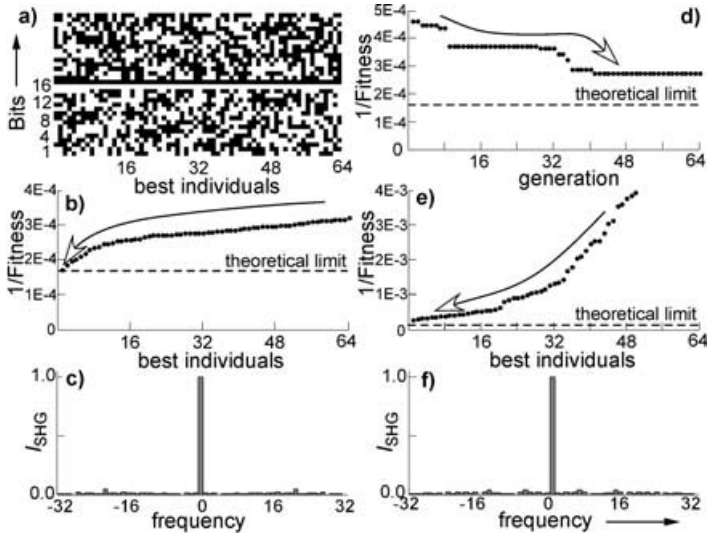

Figure 25. Exhaustive calculation and GA search for the phase that produces a narrow two-photon excitation using 32-bit phase functions. a) The 64 best individuals from the full set of calculated phases, sorted by their fitness, b) the fitness of the 64 best phases, c) the global optimum solution for this problem, d) progress of the GA, e) fitness of the 64 solution found during the last GA generation, f) the best result produced by the GA search.

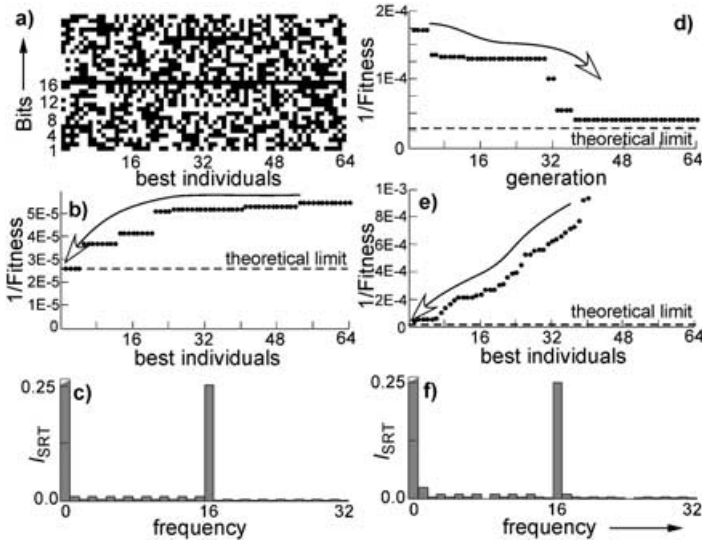

Figure 26. Exhaustive calculation and GA search for the phase that produces selective ISRS using a 32-bit phase function. a) The 64 best individuals from the full set of calculated phases, sorted according to their fitness, b) the fitness of the 64 best phases, c) the global optimum solution for this problem, d) progress of the GA, e) fitness of the 64 solutions found during the last GA generation, f) the best result found by the GA search.

The finesses of the 64 best phases in the last generation are plotted in panels (e) of Figures 24–26. The best results found by the GA search are shown in panels (f) of Figures 24–26. Compared to the optimal solution shown in panels (c) of Figures 24–26, the solution found by the GA is good but not excellent. The full size of the search space for the 32-bit problem was $N_s = 2^{N/2} = 65{,}536$. With the GA we explored $N_e = (N_a)^4 = (N/4)^4 = 8^4 = 4{,}096$ combinations, covering $N_e/N_s = 1/16$ of the search space, and in all cases found solutions which are close to the global solution. N increases exhaustive calculation is problem and only GA searches become practical.

We applied the GA search to these problems using 64-bit binary phase functions. Now the search space is of the size $N_s = 2^{N/2} = 2^{32} = 4 \times 10^9$. We increased the number of parents, the size of the population, the length of evolution and the number of catastrophes by a factor of two, because the average number of bits which are different from the best result is $N_a = 16$ now. Sampling of the overall search space by the GA is now only $N_e/N_s = (N/4)^4/2^{N/2} = (16)^4/2^{32} \approx 10^{-5}$. The exponential expansion of the search space also increases the number of relatively good solutions. The 256 steps of evolution for the three tasks are shown in panels (a–c) of Figure 27. The fitness of the 256 best individuals in the population for the last generation is shown on panels (d–f) of Figure 27. The best solutions found by the GA results are shown in panels (g–i) of Figure 27. The GA solutions are good and can be used for selective excitation. We definitely do not find the globally best phase for all three tasks. This is clearest in the first case where we wanted to find the TL pulse solution.

Next we present the results obtained using a GA to search the 32-bit space and compare the GA solutions with those obtained by exhaustive search. We used the same GA for all tasks, defining the population size and the number of parents in terms of the average number of changeable bits $N_a = N/4$. The evolution of the GA toward a solution is plotted as a function of generation in panels (d) of Figures 24–26. Note that in 64 generations the GA does not converge on the theoretical limit.

The tasks fit the description of a frustrated problem, characterized by a rough landscape where local maxima are many, steep, and narrow. This is easily seen from Figure 16e (narrowed spectral SHG) and Figure 23b (sharp ISRS) where there are a few good solutions surrounded by extremely large numbers of bad solutions. In these cases with polynomial GA searches are difficult and convergence on local solutions occurs. To prevent GA search from converging on local solutions, we periodically applied a total of N_a catastrophes to the GA population, in which we kept only N_a parents and generated a new population of random individuals. Despite this effort, the GA failed to find the theoretical optimal solution.

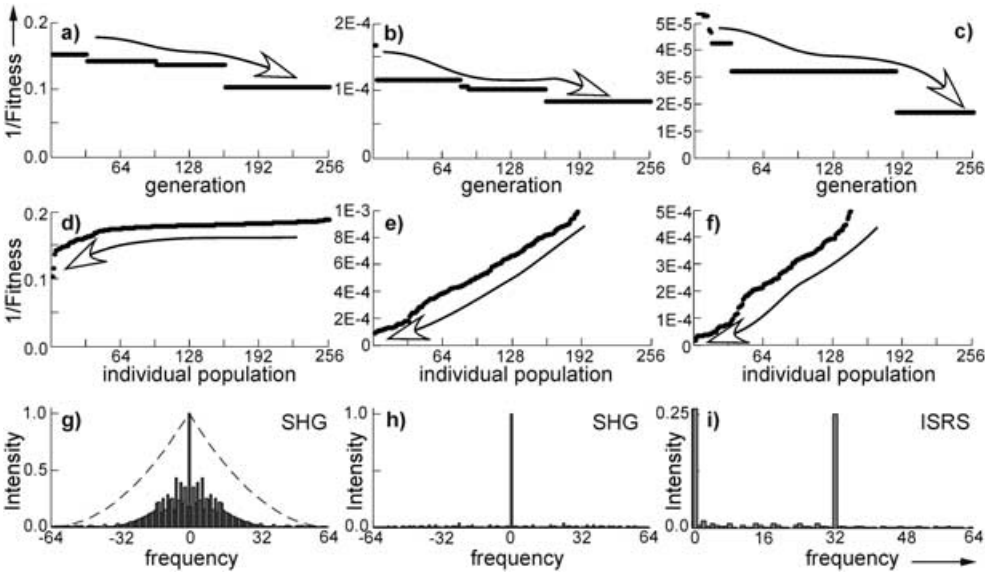

Figure 27. GA search for the optimum integrated SHG, narrowed SHG and selective ISRS using 64-bit phase functions. (a–c) Progress of GA, (d–f) fitness in the last generation, (g–i) the best solutions found by the GA.

To reach this solution we need to use a more sophisticated GA or a supercomputer with at least $N_s/N_e \approx 10^5$ more resources to carry out the exhaustive search.

The tasks become even more complicated if we use 128 or 1024 pixels. The binary search space size increases to 10^{19} or 10^{154} even after taking into account the internal symmetries. These are big search spaces, but they are minuscule compared to the task of optimization of 100 amplitudes and 100 phases for 128 pixels $(100\times100)^{128}=10^{512}$ which people have tried to explore using a GA in a slow experimental setting. Many scientists are now incorporating a new pulse shaper available with 640 pixels, having a search space of size 10^{2500}. It will likely be impossible to make useful GA progress in a search space of this size for all but the most convex of problems, unless one restricts the size of the search space. The most significant problem is that there is a very large number of phases that have the same ϕ''. Because nonlinear processes depend on ϕ'', it is important to eliminate this form of redundancy.

We have shown that for some cases a mathematical solution exists, especially when using BPS, because similar problems have been addressed for encoding information and number theory. We have also illustrated that in the absence of a rational solution, a GA search using BPS can efficiently produce an acceptable solution. Finally, we show that even in the simplest case of maximizing the total SHG, a GA may not find the optimum solution. Experimentally, this case corresponds to reducing the phase distortions in a pulse to obtain transform-limited pulses.[23–46, 124] For this task, the use of contextual operators such as smoothing (when the final result is expected to be a smooth function) greatly enhance the quality of the final result.[3]

7. Some Applications of MII

7.1. Spectral Phase Characterization Using the Multiphoton Intrapulse Interference Phase Scan (MIIPS) Method

Here we present one of the first applications to be derived from MII. The goal is to achieve accurate spectral phase characterization and compensation to obtain TL pulses. Theoretical analysis and experimental results demonstrate that the typical deviations of global methods such as frequency-resolved optical gating (FROG) are about 0.1–0.05 rad across the spectrum of 10 fs pulse.[125] Interferometric methods (such as spectral phase interferometry for direct electric-field reconstruction—SPIDER) are more local and show better accuracy[125] but these methods depend on interferometry, which requires precise alignment and stability of the setup.

Two-photon processes have their corresponding maximum efficiency where the spectral phase is globally *anti*-symmetric.[75,76] When a sinusoidal phase is scanned across the spectrum using a phase shaper, the local maximum of SHG that is obtained by the shaped beam follows the point where the second derivative of phase function equals zero (see Figure 7 with analytical and numerical solutions). It is possible to use this local dependence to develop an accurate method for spectral phase characterization.[98, 100]

The idea of MIIPS is to introduce a known function $f(\omega)$ such that the total phase is a sum of the unknown phase distortion and the known function. The Taylor expansion of this sum is given in Equation (30):

$$\varphi(\omega+\Omega)+\varphi(\omega-\Omega)=2\varphi(\omega)+\varphi''(\omega)\Omega^2+\ldots +\frac{2}{(2n)!}\varphi^{2n'}(\omega)\Omega^{2n} \quad (30)$$

We see that the odd terms $\phi'\Omega$, and $\phi'''\Omega^3$ in the sum vanish and have no effect on the SHG signal amplitude at 2ω. To first approximation, the SHG depends only on the second-order term and is maximum when the second-order derivative of the phase distortion $\phi''(\omega)$ equals 0. The SHG signal at a particular frequency is maximized when the phase function $f(\omega)$ locally compensates the unknown phase $\phi(\omega)$ being measured such that [Eq. (31)]:

$$\phi''(\omega)=\phi''(\omega)+f''(\omega)\rightarrow 0 \quad (31)$$

To measure the unknown phase modulation we can parameterize the function $f(z,\omega)$. We scan the parameter z and measure the SHG spectrum as a function of the scanned parameter SHG(z,2ω). From these spectra we obtain a 2D plot for SHG (z,2ω), from this 2D plot (see Figure 28) we can draw lines through the maxima that map $z_{max}(\omega)$, and find the second derivative of the unknown phase because we know a priori the function we introduced $f(z_{max}(\omega),\omega)$ in Equation (32):

$$\phi''(\omega)=-f''(z_{max}(\omega),\omega) \quad (32)$$

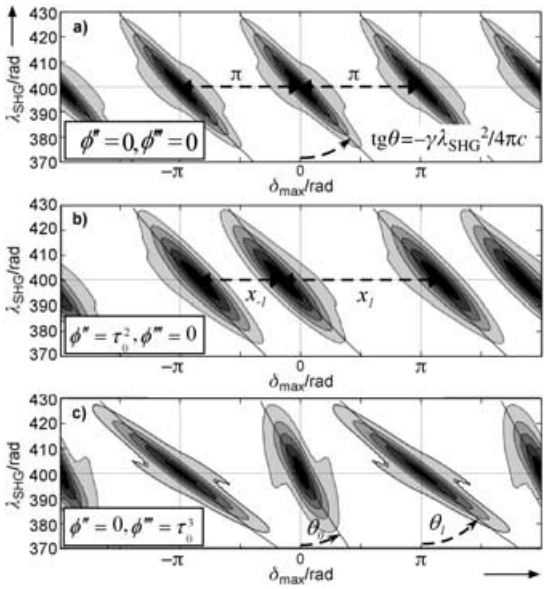

Figure 28. Simulation of MIIPS measurements for TL and chirped pulses. The horizontal axis corresponds to δ, the phase parameter that is scanned according to Equation (33). The vertical axis corresponds to the wavelength of the SHG signal. The darker the contour, the higher the SHG signal detected. (a) MIIPS trace for TL pulses. (b) MIIPS trace for the positive quadratic spectral chirp. (c) MIIPS trace for positive cubic spectral chirp. Notice that cubic chirp changes the angle of the SHG features.

The phase of the pulse across the whole spectrum $\phi(\omega)$ can be retrieved by integration of ϕ''. The constants of integration are taken to be zero such that constant phase and linear terms in the phase modulation at the carrier frequency of the pulse are zero.

We typically use a sinusoidal function as reference [see Eq. (33)]:

$$f(\delta,\omega) = \alpha \sin(\gamma(\omega-\omega_0)-\delta) \tag{33}$$

where α, γ, ω_0 are fixed parameters and phase shift δ is scanned parameter. The sine function is practical because its second derivative is a sine function as well. In this case the retrieved second derivative of the measured phase function is shown in Equation (34):

$$\phi''(\omega) = \alpha\gamma^2 \sin[\gamma(\omega-\omega_0)-\delta_{\max}(\omega)] \tag{34}$$

There are multiple solutions (index n) of Equation (34)) for all values of parameters α and γ or $\omega_{cmax}(\omega_c)=\omega_c$. Detuning $\omega_{cmax}(\omega)-\omega$ characterizes deviations from TL. Because we use a periodic reference function $f(\omega)$ we define the phase shift $\delta = \gamma(\omega_c-\omega_0)$ as the scanned parameter [Eq. (35)]:

$$\delta_{\max}(n,m) = \gamma(\omega-\omega_0)-(-1)^n \arcsin(\mathrm{mod}(\phi''(\omega)/\alpha\gamma^2,1)) + n\pi$$
$$n = 0, \pm 1, \pm 2 \ldots \tag{35}$$

In Figure 28, we plot these lines on top of the calculated SHG spectrum in the $\delta-\lambda_{SHG}$ plane.

For a TL pulse $\delta_{\max}(\omega)$ is a set of parallel lines separated by π [Eq. (36)]:

$$\delta_{\max}(n,\omega) = \gamma(\omega-\omega_0) + n\pi, \;\; n = 0, \pm 1, \pm 2 \ldots \tag{36}$$

In the first example, we show the calculated MIIPS 2D traces for pulses with $\tau_0 = 10$ fs and a Gaussian spectrum centered at 800 nm. The first panel, see Figure 28a, corresponds to TL pulses. Notice the parallel lines separated by π. A quadratic distortion, $\phi'' = \tau_0^2$, shown in Figure 28b, changes the spacing between the $\delta_{\max}(\omega)$ lines. A cubic phase $\phi''' = \tau_0^3$, shown in Figure 28c, changes the slope of the lines. A change in the sign of the chirp causes a change in the direction of the observed changes in the $\delta_{\max}(\omega)$ lines.

In Figure 29 we show a pulse with a combination of quadratic and cubic spectral phase distortion is compensated and restored to TL using MIIPS. In Figures 29a–29h we illustrate four iterations of the MIIPS method. Figures 29a–29d show the dependence of the SHG intensity as a 2D plot in the $\delta-\lambda_{SHG}$ plane for the pulse. The two lines (red and green) drawn through the local maxima correspond to $\delta_{\max}(0,\omega)$ and $\delta_{\max}(1,\omega)$ and were used to calculate the second derivative of the phase in the first iteration $\phi''^{\,1}$ with Equation (37):

$$\phi''(\omega) = -\frac{1}{2}\alpha\gamma^2 \begin{bmatrix} \sin(\gamma(\omega-\omega_0) - \delta^0_{\max}(\omega)) \\ +\sin(\gamma(\omega-\omega_0) - \delta^\pi_{\max}(\omega) \end{bmatrix} \tag{37}$$

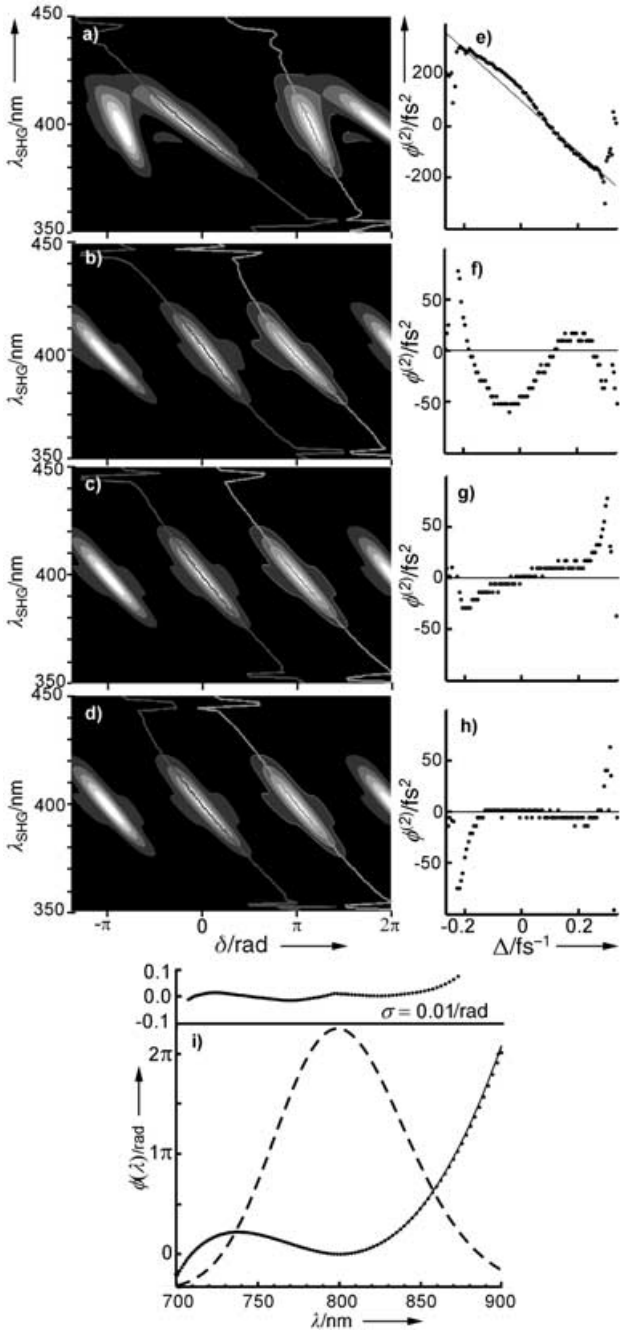

Figure 29. Calculated MIIPS traces for a 10 fs pulse with quadratic and cubic chirp. Panels (a–d) show the changes in the MIIPS trace as a function of iteration and compensation. Panel (e–h) show the residual phase for each iteration. Panel (i) shows the retrieved phase (•••••), the exact phase (——) and the residual phase after four iterations.

In Figure 29e we plot the result of the first iteration together with the exact line for the second derivative of phase. We see that even the first iteration gives a pretty good approximation. To eliminate the error in the first approximation, the retrieved phase $-\phi^{\mathrm{I}}$ was incorporated in the shaper to compensate the measured phase and a second iteration was carried out. Results for SHG, $\delta_{\max}(\lambda)$ lines and the retrieved second de-

rivative of the phase for the subsequent iterations are presented in Figure 29b through Figure 29h. We can see that the last iteration (ϕ''^{IV}) achieves the limit of zero phase distortion within the 710-870 nm spectral region. The "digital noise" of the retrieved ϕ'' is proportional to the step in δ scan and equal to $\alpha\gamma^2 4\pi/N$, where N is number of steps in the scan. Finally, the retrieved phase derivative is the cumulative sum of all the iterations as shown in Equation (38):

$$\phi_{\text{measured}} = \phi^{I} + \phi^{II} + \cdots + \phi^{N} \quad (38)$$

Deviations from the programmed phase distortion lie in the milliradian range with dispersion of 0.01 rad. To compare the retrieved phase with the programmed phase we should remember that the method is not sensitive to the common constant and linear phase distortion. This fact was taken into account when we made a plot of the measured and the programmed phase to minimize the linear term in the deviation. When analyzing experimental data, we can subtract any linear term from the retrieved phase function to minimize the range of phases that can be programmed in the pulse shaper.

The second example considers self-phase modulation. We simulate the MIIPS measurements for Gaussian pulses with duration $\tau_0 = 30$ fs and $\phi(t) = -0.5\pi \cdot I(t)$. If the phase distortion is 0.5π, the spectrum of the pulse is slightly broadened and wings of the spectrum cover the range from 600 nm to 900 nm. Four iterations of MIIPS (using $\alpha = \pi$ and $\gamma = 10$ fs) are presented in Figures 30a–30h. In this case, the second derivative of the spectral phase is sharp and is in the range from -550 fs^2 to $+400$ fs^2, which is larger than the parameter $\alpha\gamma^2$. As shown in Figure 30, the first iteration result ϕ''^{I} (dots) is significantly different from the phase derivative of the measured pulse (line). MIIPS retrieves the main trend of the derivative and after a few iterations obtains a near TL pulse (parallel lines on the 2D SHG maps), indicating accurate phase retrieval and compensation. The comparison of the retrieved phase with the programmed phase is shown in Figure 30i. After four iterations, the standard deviation measurement is less than 0.05 rad even at the edges of the spectrum.

As we see from these examples, iterative MIIPS efficiently reaches TL pulses and accurately measures spectral phase.[98, 100, 126] We simulate experimental measurements of TL pulses with noise added to the SHG 2D map. Because MIIPS is sensitive to local phase properties, we are able to do some smoothing of the data. Results for the level of noise with normal dispersion 0.001, 0.01, 0.1 and 1 from normalized SHG intensity are presented in Figure 31. We have compiled Table 1 in which we accumulated our theoretical and experimental knowledge of MIIPS precision. We have used the MIIPS method to measure the phase distortions of pulses that have propagated through one millimeter of biological tissue, this application pushed the limits of sensitivity and noise.[102] Additional details and experimental analysis of the performance parameters for MIIPS will be published elsewhere.[126]

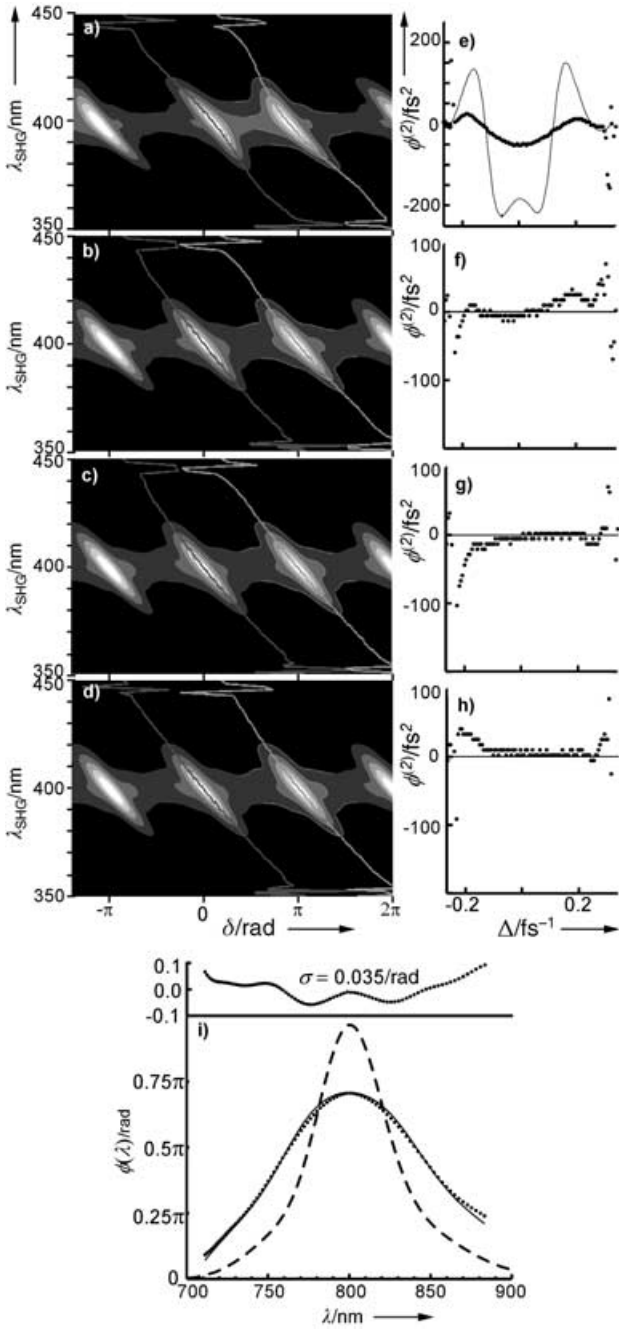

Figure 30. Calculated MIIPS traces for a 30 fs pulse with self-phase modulation. Panels (a–d) show the changes in the MIIPS trace as a function of iteration and compensation. Panels (e–h) show the residual phase for each iteration. Panel (i) shows the retrieved phase (•••••), the exact phase (——) and the residual phase after four iterations.

7.2. Selective Two-Photon Microscopy

Presently there are two methods based on coherent control that are being used for microscopy. The first method is based on CARS.[89] The shaped pulse induces the initial Raman transitions and stimulates the anti-Stokes scattering. During the shaping process, the blue end of the spectrum of the pulse is clipped, in order to reduce background photons near the signal. As this shaped beam is focused on the sample, the

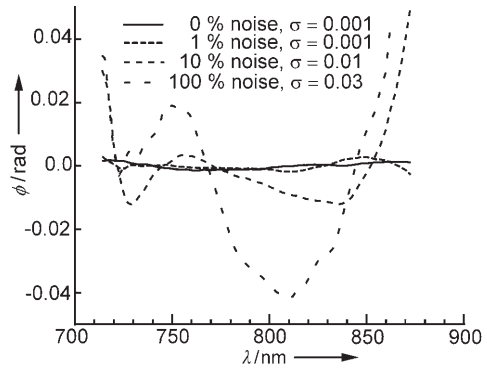

Figure 31. Calculated phases obtained by MIIPS measurement of noisy TL pulses. The different lines represent results of phase retrieval for signals with different percentages of noise. For each case we measure a standard deviation from zero. Notice that even for 100% noise, the phase measurements is accurate within 0.03 radians.

Table 1. Performance of MIIPS for different values of initial chirp and the effect of noise.

Value of max ϕ''	Standard deviation [rad]
$\phi'' < \pi\tau_0^2$	0.001
$\phi'' > \pi\tau_0^2$	0.01
Effect of noise	
$<1\%$	0.001
1%–10%	0.001–0.01
10%–100%	0.01–0.05

CARS signal is collected, providing high-resolution images that depend on the molecular identity of the sample.

Our group has demonstrated selective two-photon microscopy using the MII principles to selectively excite certain chromophores in a sample.[98,99] Whereas TL pulses excite all chromophores in the focus, a shaped pulse excites only the selected chromophores. The idea is to use MII to control the wavelength region in which two-photon transitions take place. We have shown how this method is used to selectively excite two different microscopic fluorescent beads labeled with (4′-6-Diamidino-2-phenylindole) DAPI or with AlexaFluor 430, two fluorescent chromophores that are commonly used to stain biological samples. When TL pulses are used both regions show strong fluorescence, but when shaped pulses are used, it is possible to selectively excite either of the two.[98,99] A number of chromophore pairs can be selectively excited using a similar MII approach. We have also used selective two-photon excitation to discriminate between molecules according to changes in their 2PA cross-section induced by their microchemical environment.[98,99] In those experiments we used a pH sensitive chromophore and demonstrated our ability to image acidic or basic regions. The same principle can be used for selective excitation of probes sensitive to sodium or calcium ion concentrations, for example. This method can be used for imaging microscopic as well as macroscopic biomedical samples. Selective multiphoton excitation afforded by coherent control results in additional contrast and better differentiation.

7.3. Selective Two-Photon Imaging through Tissue

The application of coherent control methods as discussed in this Review to areas of technological importance such as biomedical imaging requires that phase-modulated pulses propagate through tissue without losing their properties. Certainly scattering leads to a loss of phase information, and scattering of a laser pulse leads to a loss of coherence. The question we address here is to what extent the phase is maintained, and how could we take advantage of coherent control methods in biomedical imaging.

Two-photon imaging through tissue has proven to yield high resolution (10 μm) images through modest (one millimeter) tissue thicknesses.[127,128] This method depends on the fact that a small portion of the photons from a pulse essentially survives without scattering. These photons, known as ballistic photons, maintain the original coherence of the pulse. When a laser pulse is focused inside tissue, ballistic photons are responsible for most of the two-photon excitation of fluorescent chromophores; hence, very high spatial resolution is maintained.

Recently, we evaluated the possibility of achieving selective two-photon excitation through scattering tissue. In particular, we wanted to determine if a binary phase function that leads to selective excitation can be used for selective biomedical imaging. For our experiments we constructed a sample that consisted of three capillary tubes filled with a pH sensitive dye in an acidic buffer solution. These capillaries were submerged in a basic buffer solution containing the same pH sensitive dye. In front of the capillaries, we placed a mask with the letters MSU for visual reference and then a 1 mm slice of chicken breast tissue was used to cover the entire sample as shown in Figure 32a. A digital picture of the sample using front and back UV illumination is shown in Figure 32b. Note that in this

Figure 32. A) Setup for the experimental demonstration of coherent control through biological tissue. Three capillary tubes with an acidic solution of HTPS were submerged in an alkaline solution of HPTS. The cell, with the letters MSU was scanned in front of the shaped laser pulse. In front of the cell a 1 mm slice of biological tissue was used to test the ability of binary phase-shaped pulses to achieve functional imaging. B) Photograph of the sample with 1 mm of biological tissue, the size is approximately 4 mm. C) Functional image obtained by subtracting the images resulting from pulses optimized for excitation of acidic and alkaline HPTS. Positive values were colored red and negative values blue. The red regions correspond the capillary tubes and the blue regions correspond with the surrounding solution.

picture, the capillaries are not observed and there is no apparent difference between the regions of different pH. The difference image obtained from plotting the signal obtained using the pulses optimized for acidic and basic solutions is shown in Figure 32c. Notice that in this case, the three capillaries with acidic solution (red regions) are clearly visible and distinguishable from the basic solution (blue regions). A more detailed presentation of this work has been published elsewhere.[102]

Our results demonstrate that the method of biological imaging can be enhanced by coherent control techniques. The number of ballistic photons available for imaging decreases exponentially with depth of penetration, but with sufficient laser intensity depths of 5 millimeters can be achieved. In these cases in particular, phase modulation is required to reduce the possibility of damaging healthy tissue by third and higher order multiphoton processes.

8. Future Possible Applications

8.1. Compensation of Phase Distortions with BPS and GA

The power of MII approaches depends on the available bandwidth of the pulses being used. The greater the bandwidth, the greater the spectroscopic range over which MII can be used. Usually, very short pulses are very sensitive to phase distortion. While it is easy to generate pulses with hundreds of nanometers in bandwidth, it is very challenging to eliminate all phase distortions and achieve a TL pulse. The question we address here is whether BPS can achieve controlled multiphoton excitation despite phase distortions. In other words, we explore the question of whether a pulse with significant phase modulation across the bandwidth can be made to generate SHG at a given frequency with the efficiency of TL pulses. We start with a spectrum that corresponds to the sum of two spectra from two 10 fs laser pulses (centered on 740 nm and 860 nm). The spectral phase has quadratic ($\phi'' = \tau_0^2$), cubic ($\phi''' = \tau_0^3$) and quartic ($\phi'''' = \tau_0^4$) distortions centered on 840 nm (λ_d), meaning that $\phi(\omega) = \frac{1}{2}10^2\,\mathrm{fs}^2(\omega-\omega_d)^2 + \frac{1}{6}10^3\,\mathrm{fs}^3(\omega-\omega_d)^3 - \frac{1}{24}10^4\,\mathrm{fs}^4(\omega-\omega_d)^4$. The spectral power and phase of such pulses are presented in Figure 33a. We introduced a binary phase and let the GA find a solution that gives the desired focusing of SHG spectrum inside a 2 nm window at 390 nm. Because the initial pulse has a significant phase distortion to begin with, the SHG spectrum without BPS is suppressed in comparison to the SHG spectrum of a TL pulse (see Figure 33b). The GA provides a good solution. There is suppression of the background (outside the desired spectral window) and there is amplification of the signal inside the desired spectral window. For the example presented in Figure 33, we used the simplest GA with only mutations and one surviving parent. A more sophisticated GA would have provided an even better solution, perhaps with the maximum SHG reaching TL level and a better suppression of the background. With this demonstration, we conclude that the BPS method can be useful for controlling multiphoton spectroscopy with extremely broad band pulses that are typically generated using super continuum.[124] We should point out that the binary phase function used to optimize a process with a phase distorted pulse is different to the phase function that would be used for the same task with a TL pulse.

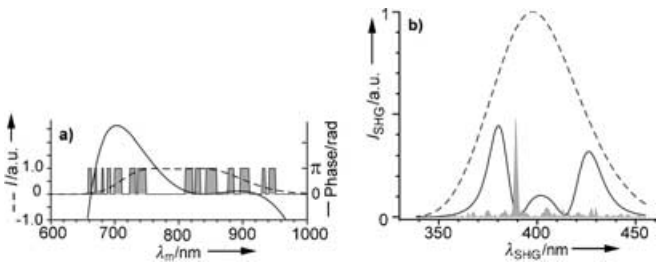

Figure 33. Spectrally narrow SHG generated from a heavily chirped pulse using a binary phase function. a) Amplitude (-----) and phase (——) of the heavily chirped pulse and the binary phase used for correction (gray), b) SHG spectrum of an equivalent TL pulse (-----), the SHG spectrum of distorted pulse (——) and the narrow SHG spectrum resulting from application of the binary phase shaping (gray).

8.2. Control of Phase and Amplitude of Multiple TPAs

The implementation of a quantum information processor has received considerable attention. The most important requirement for such a device is the ability to manipulate each quantum bit of information coherently, without loss of phase. The best ideas on how to achieve these unitary transformations are based on the use of electromagnetic radiation, either in the radio-frequency range, as in nuclear magnetic resonance (NMR) spectroscopy, or in the visible range, using coherent laser pulses. While there has been considerable progress in the use of multiple-pulse NMR spectroscopy for quantum information processing, similar methods based on laser pulses have a number of advantages. Because of the size of the quantum transitions, optical methods are eight orders of magnitude faster and are 10 orders of magnitude less prone to thermal noise.[129,130]

Using BPS we can define the sign of the electric field amplitude: when $\phi = 0$ the sign is positive and when $\phi = \pi$ the sign is negative. Multiphoton spectra also have a well-defined sign. For example, a TL pulse produces an SHG field with constant phase, or we can say positive sign across the whole spectrum. Fundamental pulse with binary modulated phase can generate a multiphoton effective field with a complex shape. The phase or sign of the SHG field depends on the local symmetry of the binary phase. If the phase is symmetric about a particular frequency then the SHG phase is 0 or 2π, and the sign of the SHG field is positive. If the phase is antisymmetricabout a particular point then the sign of the SHG field is negative.

Phase modulation can be used to generate SHG with two spectral components having a well-defined phase sign between them. To generate two components with opposite signs the fundamental spectra must have some symmetry properties. To generate a positive phase feature in the SHG at $-\Delta$ and a negative one at $+\Delta$, the fundamental phase must be symmetric around point $-\Delta/2$ and antisymmetricaround $\Delta/2$.

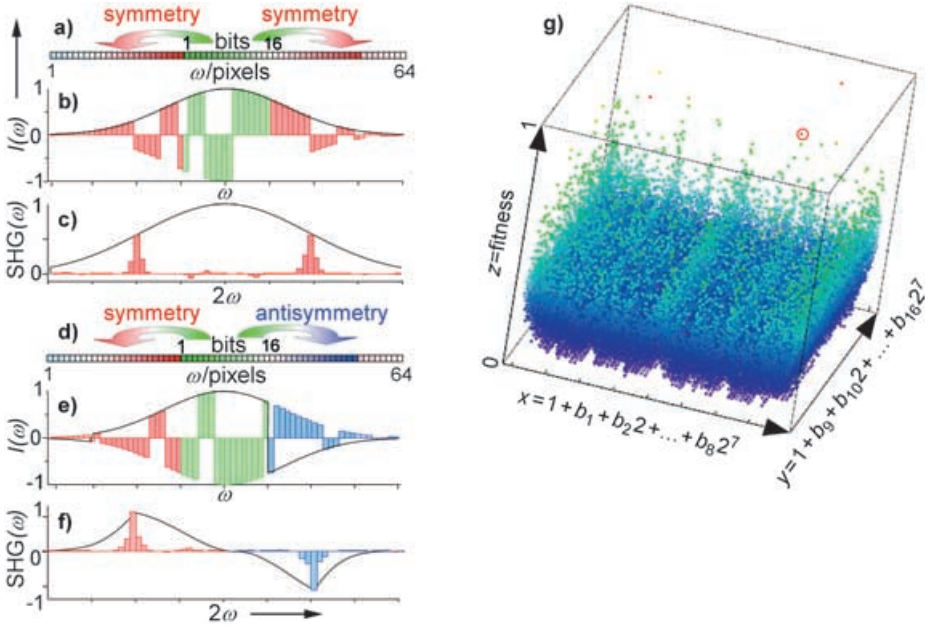

Figure 34. Phase control of two narrow SHG peaks using symmetric (a, b) and antisymmetric(d, e) binary phase shaping. The resulting SHG spectrum multiplied by the phase is shown for both cases (c) and (f). Notice that in (c) both peaks have positive phase but for (f) they have opposite phase. g) Three-dimensional representation of the search space, corresponding to the generation two peaks with opposite phase for all possible binary phase functions position on the *x*–*y* plane, depends on the phase as shown on the axis label. Note that there are very few good solutions.

To construct such phase we use the central 16 pixels of the SLM (see Figures 34a and 34d). We achieve the desired symmetric and antisymmetricphase symmetries by reflection and anti-reflection of the phase in the central 16 pixels. To generate a broad spectrum SHG with the same sign we use TL pulses (Figure 34c, black line).

To find a phase that will generate an SHG spectrum with narrow lines we explore all 2^{16} possible phases in the central part of spectra. The criteria of fitness is the total intensity in a small window around the maxima $2\omega_0 \pm \Delta$. In Figure 34g, we plot the entire search space and fitness for all possible phases (for the case *anti*-phase SHG spectra, Figures 34e and 34f). Most of the 65536 possible solutions have a small fitness; only 4 of them reach the maximum (see Figure 34g red points), and there are only a few hundred solutions that are good (Figure 34g, green points). From these figures we conclude that the task of generating sharp SHG lines with well defined phases can be solved, but is hard. Good solutions are rare in an ocean of bad solutions. This task can be categorized as a needle in a haystack, similar to that shown in Figure 15. Any gradient method to find the optimum solution will fail and only a sophisticated learning algorithm,[3,131] designed using prior knowledge of the problem and trends, can hope for even limited success.

The approach used here to generate multiple narrow peaks with well-defined phase can be used to explore the experimental implementation of quantum gates, where coherent transitions in semiconductor quantum dots or isolated atom are required. We predict that the use of nonlinear optical transitions with well defined phase and amplitude will have advantages over traditional resonance excitation. Two-photon excitation will provide better spatial resolution and prevent thermal excitation of the substrate.

8.3. Coding of Information Using MII and BPS

Here, we explore the possibility for generating a prescribed SHG spectrum with well-defined positions of maxima and minima. In particular, we consider encoding a message using phase and using the SHG spectra to decode the message. If at some frequency the SHG power is above some level, we say that value of the decoded bit is one; if the power is below a certain level then the decoded value is zero. To encode an *n*-bit message one needs 2^n pixels. In Figure 35, we show a) the grouping of the pixels b) the binary functions and c) the resulting SHG spectra to encode a 3-bit message. Preliminary estimation shows that it is possible to encode an *n*-bit

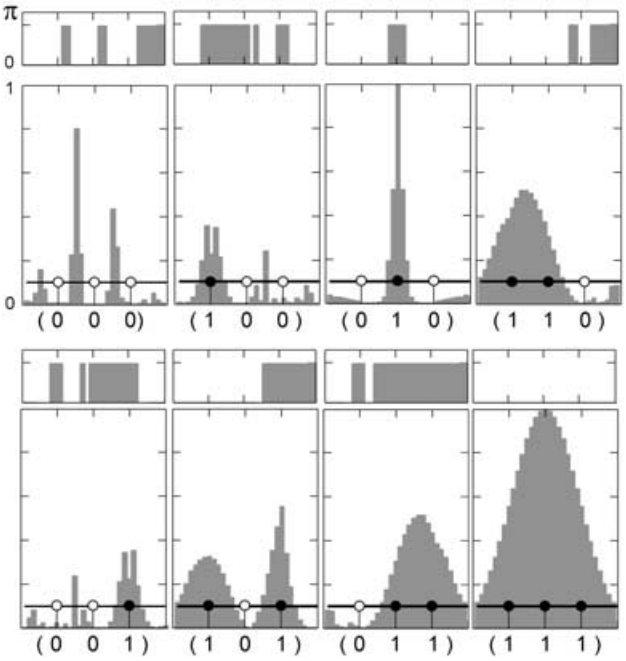

Figure 35. Coding of information with binary shaped pulses. Each binary phase function (top) encodes a 3-bit byte of information. For each case the resulting SHG spectrum which converts phase to amplitude and the corresponding string of zero and one digits are shown.

message with an SLM having $4\times n$ pixels. For example, to make the message secure Alice can put an additional binary phase modulation (key) on her SLM and send to Bob the encoded and encrypted fundamental pulse. Bob can read the message only if he has the key, which is added in his SLM. Upon generating the SHG he gets the correct message. If Eve wants to read the encoded and encrypted message but does not know the key she will see a very different pattern than Bob. Security in this case is provided by the fact that the resulting SHG spectra are very sensitive to the phase of each of pixel across the entire spectrum. This is why the search spaces analyzed for specific examples in the previous sections had few good solutions in an ocean of bad solutions. Finding the encryption key would be a very difficult task. This result could be used for building of new type of secure fast communication, one that utilizes the entire spectrum, as opposed to the single frequency method proposed by Zheng, Weiner and coworkers.[78,79] Because the pulse after BPS is longer, self phase modulation, which can distort pulses as they travel through optical fibers, will be suppressed.

9. Conclusions

The fact that the phase of an electromagnetic field affects nonlinear optical processes induced by the field has been known for a long time; however, only recently are we beginning to fully understand the connection between the two. This claim can be supported by the fact that pulse shapers have been available for almost two decades, but efforts are just beginning to define a comprehensive approach towards laser control.

Laser control problems have usually been classified into two main groups, those that are intuitively tractable, such as the two-photon excitation of an atom, and those that have been outside our ability to comprehend, such as the controlled photofragmentation and ionization of a large organic molecule. Experimentally, both of these cases have been addressed with very remarkable success. What remains is to formulate a general understanding that allows us to successfully plan and carry out experiments that are of intermediate complexity. To this end we embarked on a systematic exploration of the role of phase in nonlinear optical excitation.

The pulse shaper, having hundreds of pixels capable of controlling phase and amplitude, can provide so many different output fields that it is impossible to explore all of the possible outcomes. In response to this overwhelming size of search space, some type of restriction seems to be required. Which is the most logical approach? Our goal in Section 1 of this Review was to narrow down the possibilities by elimination. We demonstrated that amplitude modulation leads to an overall loss of photons and does not lead to desirable results. Similarly, we demonstrated that phase modulation needs a nonvanishing second derivative to properly affect nonlinear optical processes. An ideal function with this requirement and with the advantage that it does not diverge is the sine function. There are a number of very interesting results in the literature where sinusoidal functions were used for control.[67] Our analysis indicates that in some spectral regions one would like to have a much faster rate of phase change to achieve better suppression of unwanted nonlinear processes.

The search for a pulse-shaping approach with a reduced parameter space has led us to the conclusion that phase shaping using only two phase values provides an excellent alternative that is perhaps the optimum solution to most control problems. BPS has outperformed other methods in our experiments and calculations, sometimes by orders of magnitude. For simple problems, such as two or four-photon nonlinear optical processes, BPS allows us to consider rational solutions, such as those inspired by a Fresnel lens. Ultimately, even with BPS we have found that reaching the optimum solution for a particular case requires an exhaustive calculation, which can presently be carried out for 32 pixels. The use of BPS reduces a GA's search space by hundreds of orders of magnitude. This reduction leads to a more thorough exploration of the search space, to better chances of finding an optimum solution, and to the possibility of using a greater number of pixels across the spectral bandwidth (better resolution).

BPS has an important advantage in that it is the first pulse-shaping method that allows us to visualize the search space of a laser control problem. Until recently, the multidimensionality and the vastness of the search space prevented any form of representation. With BPS, we are able to plot the search space and to confirm many of the suspected features, namely, that in most cases there is more than one good solution. Recently, Rabitz et al. wrote an article on the nature of the search space.[116] In particular, the report is relevant to unrestricted (phase and amplitude) laser control of a quantum mechanical system. Rabitz has observed that each problem has a large number of solutions. More interestingly, he found that the majority of the solutions are excellent solutions, namely, that there are no intermediate solutions. His conclusion is that one should not worry about a GA converging on a local solution that is inferior compared to the global solution of the problem. This is a very significant finding because experimentally one can only sample an extremely small portion of the search space. Based on Rabitz's assertion, if the program finds a solution, it must be as good as any solution possible for that system. We have found in the cases treated here, and under the restriction of binary phase shaping, that indeed there are many solutions to every problem. However, we also find that the number of intermediate solutions is much greater than the number of good solutions. We also find that in cases where there are only one or two solutions, such as maximizing SHG conversion using BPS, the system converges on intermediate solutions and never finds the unique maximum. Surely, there is a great difference between the control of a quantum mechanical system when the electric field is an arbitrary continuous function in time, and our case where the field is first partitioned into pixels and then restricted to only two values. Perhaps the continuity in the search space considered by Rabitz provides the search algorithm a smooth gradient towards the solution. Once the search space is severely restricted, this gradient may be lost.

From the stated observations, a strategy for laser control begins to emerge. Initiate the search by using a small enough

number of active pixels such that an exhaustive search can be carried out using BPS in a practically short time, for example 16 pixels. Plotting this search space allows the experimenter to detect symmetries. Using the symmetry one can increase the number of active pixels by a factor of two or four and carry out another exhaustive search taking advantage of the reduced dimensionality afforded by symmetry. If one no longer finds symmetry in the new search space, then a GA approach can be used to further refine the search. For this step, we increase the number of pixels and set the parameters of the GA keeping in mind that the number of parents should be proportional to the number of active pixels. In our laboratory, we have a pulse shaper with 128 pixels, and we can optimize any nonlinear optical process, as shown here.

As we enter an era where phase control of nonlinear optical processes becomes robust and predictable, a number of applications begin to emerge. We have discussed such applications in the form of laser pulse characterization, selective microscopy, and biomedical imaging. We have also explored some future possible applications such as the use of pulse shaping for controlling multiphoton transitions induced by ultrabroad bandwidth pulses, using shaped pulses for quantum computing purposes and using BPS for secure communications. A number of groups are already working in these areas.

An area that is virtually absent in this Review is coherent control in the strong-field regime. Some of the most exciting results in the field of laser control have involved strong fields, we reviewed some of these in the introdution. Scully et al. have proposed the use of FAST-CARS, a method using shaped pulses for the identification of biological agents.[132] Results from this challenging task are still forthcoming.[133]

It is fair to ask if any of the conclusions reached here applies to strong fields. To answer this question we first return to the size of the search space and the need to reduce it to a manageable size. Experimental constraints limit the rate at which one can try solutions to 10^7 per day; therefore, the search space needs to be reduced significantly. We have used binary phase shaping for strong field control of chemical reactions,[103] and indeed the intensity of the different *m/z* values depends on the binary phase functions. The large differences observed (between 30-300%) in the intensity of fragment ions in the mass spectrum are highly reproducible. By combining the accurate phase characterization offered by MIIPS and binary shaping we have devised a reproducible and multidimensional analytical method for chemical agent identification purposes.[103]

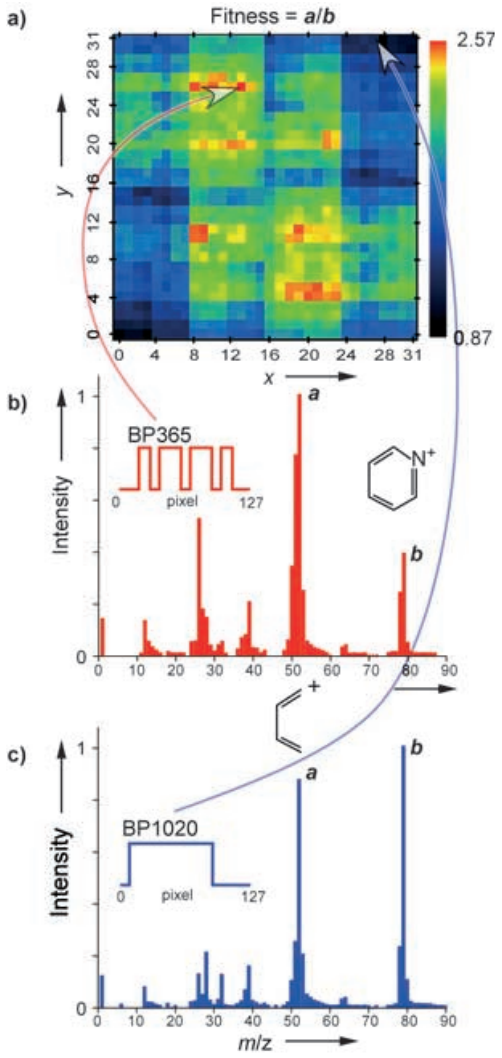

Figure 36. Experimental search space map for the strong-field control of pyridine ionization versus loss of HCN. The map (a) shows the regions where the fitness (*a/b* ratio) is highest (red) or lowest (black). Panels (b) and (c) show the experimental mass spectrum obtained with binary phase *BP*365 and *BP*1020. Each 10-bit binary-phase number is given by $BP = b_0 2^0 + b_1 2^1 + b_2 2^2 + b_3 2^3 + b_4 2^4 + b_5 2^5 + b_6 2^6 + b_7 2^7 + b_8 2^8 + b_9 2^9$, the axes in the space search map are determined by $x = b_0 2^0 + b_1 2^1 + b_2 2^2 + b_3 2^3 + b_4 2^4$ and $y = b_9 2^0 + b_8 2^1 + b_7 2^2 + b_6 2^3 + b_5 2^4$. The b_i coefficients are zero or one, to correspond the binary phase function that take the values zero and π. Notice the large difference in the relative height of peaks $a = C_4H_4^+$ resulting from HCN loss, and peak *b* which is the pyridine parent ion. Long arrows indicate the position in the map where the highest (red) and lowest (black) ratios were recorded.

An advantage of binary-phase shaping is that we can map the search space as discussed herein. In Figure 36 we present the experimentally recorded search space for the binary phase control of pyridine ionization versus loss of HCN under strong field excitation. The results were obtained using binary phase-shaped 130 μJ pulses focusing on 10^{-5} Torr pyridine vapor under fast-flow conditions. Notice that the fitness, calculated as the ratio of peaks *a* (*m/z* 52) and *b* (*m/z* 79) can be controlled from 0.87 to 2.57. In panels 36b and 36c we show the mass spectrum recorded for the largest and smallest ratios, and their associated binary phase. The search map shows inversion symmetry, this is because addition of π to a phase function gives an equivalent phase function. We see that transform-limited pulses, the bottom left and the upper right corners, lead to small *a/b* ratios where less fragmentation is observed. There seems to be more than one optimum solution. We are beginning to learn what properties of the pulses cause the most fragmentation, and we are also exploring different methods to map the information that is recorded in these experiments. This information will be published elsewhere.

In conclusion, progress in the field of laser control has accelerated considerably in recent years given the availability of reli-

able femtosecond lasers and pulse shapers. A general understanding of the effect of phase on nonlinear optical transitions is solidifying, allowing the development of applications in diverse fields. There still remain a number of challenges, especially in the area of strong-field laser–molecule interactions. A more general understanding as to the nature of the search space will greatly benefit these efforts, especially when experimental constraints limit the total number of experiments that can be carried out. From a small sample of results it may be possible to determine if the search space is rich in good solutions, or not. It may also be possible to determine if the search space has some symmetry that can be used to find the optimum value with a minimal number of experiments. The results shown here illustrate how close interaction between theory in the form of physical insights and number theory can be used to solve some of the challenges in coherent control and provide some of the first calculated search maps from coherent control search spaces. Our group is continuing to explore these fundamental aspects as well as developing applications for this emerging field.

Acknowledgments

Our research on coherent control has been supported primarily by the Chemical Sciences, Geosciences and Biosciences Division, Office of Basic Energy Sciences, Office of Science, U.S. Department of Energy. The National Science Foundation has provided funds for our work on four-wave mixing and related methods to observe and control molecular dynamics, and for the development of MIIPS. Their funding is gratefully acknowledged. MD is a Camille Dreyfus Teacher-Scholar. We wish to thank Jonathan Hall and Matt Comstock for many stimulating discussions. The efforts and dedication of K. A. Walowicz, I. Pastirk, J. Dela Cruz, and M. Comstock, referenced in this Review, have made our contributions possible. We also thank M. J. Kangas and Janelle Shane for providing the experimental search space map for the strong field control of pyridine ionization versus fragmentation. We thank J. Gunn, M. J. Kangas and A. L. Smeigh for proofreading this manuscript.

Keywords: femtochemistry · laser spectroscopy · mass spectroscopy · pulse shaping · Raman spectroscopy

[1] A. D. Bandrauk, Y. Fujimura, R. J. Gordon, *Laser Control and Manipulation of Molecules, Vol.* 821, American Chemical Society, Washington, **2002**, p. 371.
[2] N. E. Henriksen, *Chem. Soc. Rev.* **2002**, *31*, 37 – 42.
[3] T. C. Weinacht, P. H. Bucksbaum, *J. Opt. B* **2002**, *4*, R35-R52.
[4] G. Roberts, *Philos. Trans. R. Soc. London Ser. A* **2002**, *360*, 987 – 1021.
[5] S. A. Rice, S. P. Shah, *Phys. Chem. Chem. Phys.* **2002**, *4*, 1683 – 1700.
[6] T. Brixner, G. Gerber, *ChemPhysChem* **2003**, *4*, 418 – 438.
[7] D. Goswami, *Phys. Rep.* **2003**, *374*, 385 – 481.
[8] H. Rabitz, *Science* **2003**, *299*, 525.
[9] M. Shapiro, P. Brumer, *Principles of the quantum control of molecular processes*, Wiley-Interscience, Hoboken, NJ, **2003**, p. 354.
[10] M. Dantus, V. V. Lozovoy, *Chem. Rev.* **2004**, *104*, 1813 – 1859.
[11] W. S. Warren, *J. Chem. Phys.* **1984**, *81*, 5437 – 5448.
[12] C. P. Lin, J. Bates, J. T. Mayer, W. S. Warren, *J. Chem. Phys.* **1987**, *86*, 3750 – 3751.
[13] A. M. Weiner, D. E. Leaird, G. P. Wiederrecht, K. A. Nelson, *Science* **1990**, *247*, 1317 – 1319.
[14] A. M. Weiner, D. E. Leaird, G. P. Wiederrecht, K. A. Nelson, *J. Opt. Soc. Am. B* **1991**, *8*, 1264 – 1275.
[15] A. M. Weiner, J. P. Heritage, J. A. Salehi, *Opt. Lett.* **1988**, *13*, 300 – 302.
[16] A. M. Weiner, D. E. Leaird, *Opt. Lett.* **1990**, *15*, 51 – 53.
[17] D. H. Reitze, A. M. Weiner, D. E. Leaird, *Appl. Phys. Lett.* **1992**, *61*, 1260 – 1262.
[18] B. Broers, L. D. Noordam, H. B. V. Vandenheuvell, *Phys. Rev. A* **1992**, *46*, 2749 – 2756.
[19] B. Broers, L. D. Noordam, H. B. V. Vandenheuvell, *Inst. Phys. Conf. Ser.* **1992**, 223 – 226.
[20] B. Broers, H. B. V. Vandenheuvell, L. D. Noordam, *Opt. Commun.* **1992**, *91*, 57 – 61.
[21] R. S. Judson, H. Rabitz, *Phys. Rev. Lett.* **1992**, *68*, 1500 – 1503.
[22] C. J. Bardeen, V. V. Yakovlev, K. R. Wilson, S. D. Carpenter, P. M. Weber, W. S. Warren, *Chem. Phys. Lett.* **1997**, *280*, 151 – 158.
[23] D. Meshulach, D. Yelin, Y. Silberberg, *Opt. Commun.* **1997**, *138*, 345 – 348.
[24] D. Yelin, D. Meshulach, Y. Silberberg, *Opt. Lett.* **1997**, *22*, 1793 – 1795.
[25] D. Meshulach, D. Yelin, Y. Silberberg, *J. Opt. Soc. Am. B* **1998**, *15*, 1615 – 1619.
[26] T. Baumert, T. Brixner, V. Seyfried, M. Strehle, G. Gerber, *Appl. Phys. B* **1997**, *65*, 779 – 782.
[27] T. Brixner, M. Strehle, G. Gerber, *Appl. Phys. B* **1999**, *68*, 281 – 284.
[28] T. Brixner, A. Oehrlein, M. Strehle, G. Gerber, *Appl. Phys. B* **2000**, *70*, S119-S124.
[29] A. Efimov, D. H. Reitze, *Opt. Lett.* **1998**, *23*, 1612 – 1614.
[30] A. Efimov, M. D. Moores, N. M. Beach, J. L. Krause, D. H. Reitze, *Opt. Lett.* **1998**, *23*, 1915 – 1917.
[31] A. Efimov, M. D. Moores, B. Mei, J. L. Krause, C. W. Siders, D. H. Reitze, *Appl. Phys. B* **2000**, *70*, S133 – S141.
[32] A. Rundquist, A. Efimov, D. H. Reitze, *J. Opt. Soc. Am. B* **2002**, *19*, 2468 – 2478.
[33] K. Takasago, M. Takekawa, M. Suzuki, K. Komori, F. Kannari, *IEEE J. Sel. Top. Quantum Electron.* **1998**, *4*, 346 – 352.
[34] K. Ohno, T. Tanabe, F. Kannari, *J. Opt. Soc. Am. B* **2002**, *19*, 2781 – 2790.
[35] T. Tanabe, K. Ohno, T. Okamoto, M. Yamanaka, F. Kannari, *Jpn. J. Appl. Phys. Part 1* **2004**, *43*, 1366 – 1375.
[36] E. Zeek, K. Maginnis, S. Backus, U. Russek, M. Murnane, G. Mourou, H. Kapteyn, G. Vdovin, *Opt. Lett.* **1999**, *24*, 493 – 495.
[37] E. Zeek, R. Bartels, M. M. Murnane, H. C. Kapteyn, S. Backus, G. Vdovin, *Opt. Lett.* **2000**, *25*, 587 – 589.
[38] D. Zeidler, T. Hornung, D. Proch, M. Motzkus, *Appl. Phys. B* **2000**, *70*, S125-S131.
[39] M. R. Armstrong, P. Plachta, E. A. Ponomarev, R. J. D. Miller, *Opt. Lett.* **2001**, *26*, 1152 – 1154.
[40] M. Armstrong, P. Plachta, E. A. Ponomarev, J. P. Ogilvie, A. M. Nagy, R. J. D. Miller, *Appl. Phys. B* **2002**, *74*, S127-S132.
[41] A. Baltuska, T. Fuji, T. Kobayashi, *Opt. Lett.* **2002**, *27*, 306 – 308.
[42] A. Baltuska, T. Kobayashi, *Appl. Phys. B* **2002**, *75*, 427 – 443.
[43] F. L. Legare, J. M. Fraser, D. M. Villeneuve, P. B. Corkum, *Appl. Phys. B* **2002**, *74*, S279-S282.
[44] P. Baum, S. Lochbrunner, L. Gallmann, G. Steinmeyer, U. Keller, E. Riedle, *Appl. Phys. B* **2002**, *74*, S219-S224.
[45] L. Gallmann, G. Steinmeyer, G. Imeshev, J. P. Meyn, M. M. Fejer, U. Keller, *Appl. Phys. B* **2002**, *74*, S237-S243.
[46] U. Siegner, M. Haiml, J. Kunde, U. Keller, *Opt. Lett.* **2002**, *27*, 315 – 317.
[47] A. Assion, T. Baumert, M. Bergt, T. Brixner, B. Kiefer, V. Seyfried, M. Strehle, G. Gerber, *Science* **1998**, *282*, 919 – 922.
[48] M. Bergt, T. Brixner, B. Kiefer, M. Strehle, G. Gerber, *J. Phys. Chem. A* **1999**, *103*, 10381 – 10387.
[49] A. Glass, T. Rozgonyi, T. Feurer, R. Sauerbrey, G. Szabo, *Appl. Phys. B* **2000**, *71*, 267 – 276.
[50] C. Daniel, J. Full, L. Gonzalez, C. Kaposta, M. Krenz, C. Lupulescu, J. Manz, S. Minemoto, M. Oppel, P. Rosendo-Francisco, S. Vajda, L. Woste, *Chem. Phys.* **2001**, *267*, 247 – 260.
[51] T. Brixner, B. Kiefer, G. Gerber, *Chem. Phys.* **2001**, *267*, 241 – 246.
[52] R. J. Levis, G. M. Menkir, H. Rabitz, *Science* **2001**, *292*, 709 – 713.
[53] R. J. Levis, H. A. Rabitz, *J. Phys. Chem. A* **2002**, *106*, 6427 – 6444.

[54] N. H. Damrauer, C. Dietl, G. Krampert, S. H. Lee, K. H. Jung, G. Gerber, *Eur. Phys. J. D* **2002**, *20*, 71 – 76.
[55] M. Bergt, T. Brixner, C. Dietl, B. Kiefer, G. Gerber, *J. Organomet. Chem.* **2002**, *661*, 199 – 209.
[56] C. Daniel, J. Full, L. Gonzalez, C. Lupulescu, J. Manz, A. Merli, S. Vajda, L. Woste, *Science* **2003**, *299*, 536 – 539.
[57] T. Hornung, R. Meier, D. Zeidler, K. L. Kompa, D. Proch, M. Motzkus, *Appl. Phys. B* **2000**, *71*, 277 – 284.
[58] D. Zeidler, S. Frey, K. L. Kompa, M. Motzkus, *Phys. Rev. A* **2001**, *64*, 023420.
[59] T. Ando, T. Urakami, H. Itoh, Y. Tsuchiya, *Appl. Phys. Lett.* **2002**, *80*, 4265 – 4267.
[60] T. Brixner, N. H. Damrauer, P. Niklaus, G. Gerber, *Nature* **2001**, *414*, 57 – 60.
[61] T. Brixner, N. H. Damrauer, B. Kiefer, G. Gerber, *J. Chem. Phys.* **2003**, *118*, 3692 – 3701.
[62] T. C. Weinacht, J. L. White, P. H. Bucksbaum, *J. Phys. Chem. A* **1999**, *103*, 10166 – 10168.
[63] T. Hornung, R. Meier, M. Motzkus, *Chem. Phys. Lett.* **2000**, *326*, 445 – 453.
[64] T. C. Weinacht, R. Bartels, S. Backus, P. H. Bucksbaum, B. Pearson, J. M. Geremia, H. Rabitz, H. C. Kapteyn, M. M. Murnane, *Chem. Phys. Lett.* **2001**, *344*, 333 – 338.
[65] R. A. Bartels, T. C. Weinacht, S. R. Leone, H. C. Kapteyn, M. M. Murnane, *Phys. Rev. Lett.* **2002**, *88*, 033001.
[66] D. Zeidler, S. Frey, W. Wohlleben, M. Motzkus, F. Busch, T. Chen, W. Kiefer, A. Materny, *J. Chem. Phys.* **2002**, *116*, 5231 – 5235.
[67] J. L. Herek, W. Wohlleben, R. J. Cogdell, D. Zeidler, M. Motzkus, *Nature* **2002**, *417*, 533 – 535.
[68] R. Bartels, S. Backus, E. Zeek, L. Misoguti, G. Vdovin, I. P. Christov, M. M. Murnane, H. C. Kapteyn, *Nature* **2000**, *406*, 164 – 166.
[69] S. Vajda, A. Bartelt, E. C. Kaposta, T. Leisner, C. Lupulescu, S. Minemoto, P. Ros *endo*-Francisco, L. Woste, *Chem. Phys.* **2001**, 267, 231 – 239.
[70] A. Bartelt, A. Lindinger, C. Lupulescu, S. Vajda, L. Woste, *Phys. Chem. Chem. Phys.* **2004**, *6*, 1679 – 1686.
[71] B. J. Pearson, J. L. White, T. C. Weinacht, P. H. Bucksbaum, *Phys. Rev. A* **2001**, *6306*, 063412.
[72] F. G. Omenetto, A. J. Taylor, M. D. Moores, D. H. Reitze, *Opt. Lett.* **2001**, *26*, 938 – 940.
[73] J. Kunde, B. Baumann, S. Arlt, F. Morier-Genoud, U. Siegner, U. Keller, *Appl. Phys. Lett.* **2000**, *77*, 924 – 926.
[74] T. Hornung, R. Meier, R. de Vivie-Riedle, M. Motzkus, *Chem. Phys.* **2001**, *267*, 261 – 276.
[75] D. Meshulach, Y. Silberberg, *Nature* **1998**, *396*, 239 – 242.
[76] D. Meshulach, Y. Silberberg, *Phys. Rev. A* **1999**, *60*, 1287 – 1292.
[77] A. H. Buist, M. Muller, R. I. Ghauharali, G. J. Brakenhoff, J. A. Squier, C. J. Bardeen, V. V. Yakovlev, K. R. Wilson, *Opt. Lett.* **1999**, *24*, 244 – 246.
[78] Z. Zheng, S. Shen, H. Sardesai, C. C. Chang, J. H. Marsh, M. M. Karkhanehchi, A. M. Weiner, *Opt. Commun.* **1999**, *167*, 225 – 233.
[79] Z. Zheng, A. M. Weiner, *Chem. Phys.* **2001**, *267*, 161 – 171.
[80] Z. Zheng, A. M. Weiner, *Opt. Lett.* **2000**, *25*, 984 – 986.
[81] H. Wang, Z. Zheng, D. E. Leaird, A. M. Weiner, T. A. Dorschner, J. J. Fijol, L. J. Friedman, H. Q. Nguyen, L. A. Palmaccio, *IEEE J. Sel. Top. Quantum Electron.* **2001**, *7*, 718 – 727.
[82] M. Hacker, R. Netz, M. Roth, G. Stobrawa, T. Feurer, R. Sauerbrey, *Appl. Phys. B* **2001**, *73*, 273 – 277.
[83] N. Dudovich, B. Dayan, S. M. G. Faeder, Y. Silberberg, *Phys. Rev. Lett.* **2001**, *86*, 47 – 50.
[84] N. Dudovich, D. Oron, Y. Silberberg, *Phys. Rev. Lett.* **2002**, *88*, 123004.
[85] J. B. Ballard, H. U. Stauffer, Z. Amitay, S. R. Leone, *J. Chem. Phys.* **2002**, *116*, 1350 – 1360.
[86] D. Oron, N. Dudovich, D. Yelin, Y. Silberberg, *Phys. Rev. Lett.* **2002**, *88*, 063004.
[87] D. Oron, N. Dudovich, Y. Silberberg, *Phys. Rev. Lett.* **2002**, *89*, 273001.
[88] D. Oron, N. Dudovich, D. Yelin, Y. Silberberg, *Phys. Rev. A* **2002**, *65*, 043408.
[89] N. Dudovich, D. Oron, Y. Silberberg, *Nature* **2002**, *418*, 512 – 514.
[90] D. Oron, N. Dudovich, Y. Silberberg, *Phys. Rev. Lett.* **2003**, *90*, 213902.
[91] N. Dudovich, D. Oron, Y. Silberberg, *Phys. Rev. Lett.* **2004**, *92*, 103003.
[92] M. Renard, E. Hertz, B. Lavorel, O. Faucher, *Phys. Rev. A* **2004**, *69*, 043401.
[93] V. V. Lozovoy, I. Pastirk, E. J. Brown, B. I. Grimberg, M. Dantus, *Int. Rev. Phys. Chem.* **2000**, *19*, 531 – 552.
[94] B. I. Grimberg, V. V. Lozovoy, M. Dantus, S. Mukamel, *J. Phys. Chem. A* **2002**, *106*, 697 – 718.
[95] K. A. Walowicz, I. Pastirk, V. V. Lozovoy, M. Dantus, *J. Phys. Chem. A* **2002**, *106*, 9369 – 9373.
[96] V. V. Lozovoy, I. Pastirk, K. A. Walowicz, M. Dantus, *J. Chem. Phys.* **2003**, *118*, 3187 – 3196.
[97] M. Dantus, V. V. Lozovoy, I. Pastirk, *OE Magazine* **2003**, *9*, 15 – 17.
[98] J. M. Dela Cruz, I. Pastirk, V. V. Lozovoy, K. A. Walowicz, M. Dantus, *J. Phys. Chem. A* **2004**, *108*, 53 – 58.
[99] I. Pastirk, J. M. Dela Cruz, K. A. Walowicz, V. V. Lozovoy, M. Dantus, *Opt. Express* **2003**, *11*, 1695 – 1701.
[100] V. V. Lozovoy, I. Pastirk, M. Dantus, *Opt. Lett.* **2004**, *29*, 775 – 777.
[101] M. Comstock, V. V. Lozovoy, I. Pastirk, M. Dantus, *Opt. Express* **2004**, *12*, 1061 – 1066.
[102] J. M. Dela Cruz, I. Pastirk, M. Comstock, V. V. Lozovoy, M. Dantus, *Proc. Natl. Acad. Sci. USA* **2004**, *101*, 16996 – 17001.
[103] I. Pastirk, M. Kangas, M. Dantus, *J. Phys. Chem. A* **2005**, *109*, 2413 – 2416.
[104] N. Bloembergen, *Nonlinear optics*, 4th ed., World Scientific, Singapore, River Edge, NJ, **1996**, p. 172.
[105] Y. R. Shen, *The principles of nonlinear optics*, Wiley-Interscience, Hoboken, NJ, **2003**, p. 563.
[106] R. W. Boyd, *Nonlinear optics*, Academic Press, Boston, **1992**, p. 439.
[107] S. Mukamel, *Principles of nonlinear optical spectroscopy*, Oxford University Press, New York, **1995**, p. 543.
[108] D. Lee, A. C. Albtrecht, *Adv. Infrared Raman Spectrosc.* **1985**, *12*, 179 – 213.
[109] A. Baltuska, M. S. Pshenichnikov, D. A. Wiersma, *IEEE J. Quantum Electron.* **1999**, *35*, 459 – 478.
[110] A. Baltuska, M. S. Pshenichnikov, D. A. Wiersma, *Opt. Lett.* **1998**, *23*, 1474 – 1476.
[111] W. R. Zipfel, R. M. Williams, W. W. Webb, *Nat. Biotechnol.* **2003**, *21*, 1368 – 1376.
[112] J. M. Dela Cruz, I. Pastirk, M. Comstock, M. Dantus, *Opt. Express* **2004**, *12*, 4144 – 4149.
[113] J. M. Dela Cruz, *Opt. Express* **2004**, submitted.
[114] H. A. Rabitz, M. M. Hsieh, C. M. Rosenthal, *Science* **2004**, *303*, 1998 – 2001.
[115] N. Dudovich, D. Oron, Y. Silberberg, *J. Chem. Phys.* **2003**, *118*, 9208 – 9215.
[116] T. Helleseth, P. V. Kumar in *Mobile Communication Handbook: Pseudonoise sequences* (Ed.: S. S. Suthersan), CRC, Boca Raton, FL, **1999**.
[117] D. V. Sarwate, M. B. Pursley, *Proc. IEEE* **1980**, *68*, 593 – 619.
[118] J. Knauer, *Merit factor records*, http://www.cecm.sfu.ca/~jknauer/labs/records.html.
[119] J. Hall, private communication.
[120] R. Skaug, J. F. Hjelmstad, *Spread Spectrum in Communication* (Ed.: P.Peregrinus), Institution of Electrical Engineers, London, **1985**, p. 201.
[121] M. R. Schroeder, Number Theory in Science and Communication: With Applications in Cryptography, Physics, Digital Information, Computing, and Self-Similarity, 3rd ed., Springer, Berlin, **1997**, p. 362.
[122] B. Militzer, M. Zamparelli, D. Buele, *EEE Trans. Evolut. Comp.* **1998**, *2*, 34 – 39.
[123] W. H. Press, S. A. Teukolsky, W. T. Vettering, B. P. Flannery, *Numerical recipies in C. The art of Scientific Computing*, 2nd ed., Cambridge University Press, Cambridge, **1992**, p. 994.
[124] B. Schenkel, J. Biegert, U. Keller, C. Vozzi, M. Nisoli, G. Sansone, S. Stagira, S. De Silvestri, O. Svelto, *Opt. Lett.* **2003**, *28*, 1987 – 1989.
[125] L. Gallmann, D. H. Sutter, N. Matuschek, G. Steinmeyer, U. Keller, *Appl. Phys. B* **2000**, *70*, S67-S75.
[126] B. Xu, J. M. Dela Cruz, J. M. Gunn, V. V. Lozovoy, M. Dantus, *J. Opt. Soc. Am. B* **2005**, accepted.
[127] W. Denk, *Eur. J. Neurosci.* **1998**, *10*, 267 – 267.
[128] M. Wachowiak, W. Denk, R. W. Friedrich, *Proc. Natl. Acad. Sci. USA* **2004**, *101*, 9097 – 9102.
[129] W. S. Warren, *Science* **1997**, *277*, 1688 – 1689.
[130] V. V. Lozovoy, M. Dantus, *Chem. Phys. Lett.* **2002**, *351*, 213 – 221.

[131] D. E. Goldberg, *Genetic algorithms in search, optimization, and machine learning*, Addison–Wesley, Reading, MA, **1989**, p. 412.
[132] M. O. Scully, G. W. Kattawar, R. P. Lucht, T. Opatrny, H. Pilloff, A. Rebane, A. V. Sokolov, M. S. Zubairy, *Proc. Natl. Acad. Sci. USA* **2002**, *99*, 10994–11001.
[133] G. Beadie, J. Reintjes, M. Bashkansky, T. Opatrny, M. O. Scully, *J. Mod. Opt.* **2003**, *50*, 2361–2368.

Received: July 22, 2004
Revised: June 6, 2005

